DOI: 10.26599/FSHW.2026.9250992

Contents lists available at SciOpen

Food Science and Human Wellness

journal homepage: https://www.sciopen.com/journal/2097-0765

China Food Publishing Co.

Comprehensive identification and semi-quantitative profiling of 3,5,6,7,8,3′,4′-heptamethoxyflavone metabolites in rats by UHPLC-LTQ-Orbitrap mass spectrometry

Konglong Feng[a,b,†], Yilu Chen[c,†], Mingyue Song[b], Yu Song[b], Guo Liu[b], Meng Kang[b], Chi-Tang Ho[d], Hang Xiao[c,*], Yong Cao[b,*]

[a]*School of Food Science and Engineering, Foshan University, Foshan, Guangdong 528000, China*

[b]*Guangdong Provincial Key Laboratory of Nutraceuticals and Functional Foods, College of Food Sciences, South China Agricultural University, Guangzhou, Guangdong 510642, China*

[c]*Department of Food Science, University of Massachusetts, Amherst, MA 01003, USA*

[d]*Department of Food Science, Rutgers University, 65 Dudley Road, New Brunswick, New Jersey 08901, USA*

ABSTRACT: 3,5,6,7,8,3′,4′-Heptamethoxyflavone (HMF), one of the highest *O*-methyl numbers in the polymethoxyflavones, possesses various significant health benefits. However, the *in vivo* metabolic profile of HMF remains largely unexplored. In this study, a systematic identification and relative quantitation of HMF and its metabolites in rats were performed using UHPLC-LTQ-Orbitrap mass spectrometry combined with enzymatic hydrolysis. A total of 56 metabolites were tentatively identified, including 37 demethylated metabolites and 19 glucuronide conjugates of these demethylated products. Notably, all seven mono-demethylated metabolites of HMF were simultaneously detected and structurally discriminated for the first time in rats, along with other di-, tri-, tetra-, and penta-demethylated metabolites. Semi-quantitative analysis revealed that HMF underwent predominant biotransformation into mono-demethylated metabolites in rats, followed by progressive sequential demethylation of these metabolites to generate more di-, tri-, tetra-, and penta-demethylated metabolites. Demethylation and glucuronidation are the primary metabolic pathways of HMF *in vivo*. This study presents the first comprehensive elucidation of the *in vivo* metabolic profile of HMF, which is helpful for further understanding of its *in vivo* potential effective components and pharmacological mechanism.

Keywords: 3,5,6,7,8,3′,4′-heptamethoxyflavone; *in vivo* metabolites; demethylation; UPLC-HRMS/MS; metabolic profile

1. Introduction

Polymethoxyflavones (PMFs) constitute a unique class of methylated flavonoids, predominantly found in citrus peels (Figure 1A). 3,5,6,7,8,3′,4′-Heptamethoxyflavone (HMF) , one of the PMFs with the highest number of *O*-methyl groups, features seven methoxyl groups on its flavone core, located at the 5, 6, 7, 8-positions of A-ring, 3′,4′-positions of the B-ring and 3-position of the C-ring (Figure 1B)[1]. Because a

[†]Konglong Feng and Yilu Chen contributed equally to this work.
***Corresponding authors:**
Yong Cao, E-mail: caoyong2181@scau.edu.cn.
Hang Xiao, Email: hangxiao@foodsci.umass.edu.

Received 11 August 2025
Received in revised from 13 September 2025
Accepted 28 October 2025

higher degree of methoxylation often enhances biological activity, HMF has attracted growing research interest[2, 3]. Previous studies have demonstrated that HMF exhibits a range of promising bioactivities, with lipid-lowering and neurotrophic effects that are often more pronounced than those of other common PMFs like nobiletin or tangeretin[3-6]. In particular, our prior work has proved that dietary supplementation with HMF markedly ameliorates obesity and hyperlipidemia[7, 8]. However, the underlying mechanisms of these effects remain unclear. Given that the bioactivities of PMFs is closely linked to their bioavailability and often to the bioactivities of their metabolites[9-12], we hypothesize that HMF metabolites may contribute substantially to its pharmacological effects. Therefore, a thorough characterization of the *in vivo* metabolic profile of HMF is essential for elucidating their potential health benefits and mechanisms of action. Although earlier studies detected several mono- and di-demethylated metabolites of HMF along with their glucuronide conjugates in mice[13, 14], the chemical structures of these metabolites were not fully identified due to limited analytical characterization and a lack of authentic standards. Consequently, a comprehensive investigation of the *in vivo* metabolic profile of HMF remains lacking.

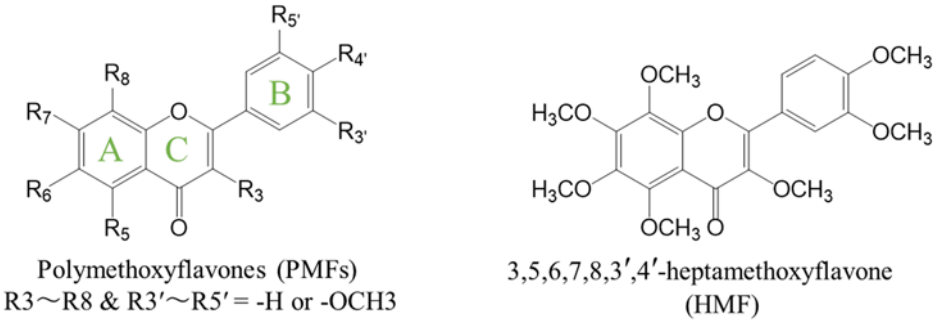

Figure 1. Chemical structures of polymethoxyflavones (PMFs) and 3,5,6,7,8,3′,4′-heptamethoxyflavone (HMF).

PMFs primarily underwent demethylation, followed by glucuronidation and sulfation *in vivo*[15, 16]. In the case of the two most common PMFs, nobiletin and tangeretin, the 3′- and 4′-positions of the B ring are the primary sites for demethylation[17-19]. In addition to the mono-demethylation pathway, both di-demethylation and tri-demethylation pathways have also been reported for nobiletin and tangeretin[10, 20, 21]. Despite extensive work on the metabolic profiles of nobiletin and tangeretin, few studies have comprehensively investigated the overall biotransformation of PMFs, including the identification of A-ring or C-ring demethylated metabolites and other various multi-demethylated metabolites. In addition, the metabolism of PMFs was affected by the number and position of the hydroxyl and methoxyl groups[21, 22]. However, the identification of HMF metabolites *in vivo* and how they differ from other PMFs, such as nobiletin and tangeretin, are still unknown and thus need further investigation. HMF is a close analog of nobiletin or tangeretin, yet it possesses the most methoxyl groups, potentially making it a more representative compound for PMFs. Therefore, understanding the metabolic profile of HMF could enhance our understanding of PMFs' biotransformation.

Utilizing mass spectrometry techniques, a greater number of phytochemical metabolites have been detected and identified both *in vitro* and *in vivo*[23, 24]. In this study, we established an effective strategy for the systematic screening and identification of HMF metabolites *in vivo*, employing UHPLC-LTQ-Orbitrap

high-resolution mass spectrometry (HRMS)/MS combined with pre-treatment with enzymatic hydrolysis, various data-acquisition and data-processing methods. A total of 56 metabolites of HMF were found and their structures were tentatively identified based on the accurate mass data acquired, diagnostic product ions (DPIs), and knowledge of PMFs' biotransformation pathways. Furthermore, we analyzed the relative abundance of all demethylated metabolites of HMF by area normalization method. Finally, on the basis of metabolite identification and semi-quantitative analysis, the *in vivo* metabolic profile of HMF was preliminarily summarized in this study.

2. Materials and methods

2.1 Chemicals and reagents.

HMF, with a purity greater than 95%, was purified according to our previous study[7]. Standard HMF (purity>98%), HPLC-grade formic acid and sodium carboxymethyl cellulose (CMC-Na) were purchased from Shanghai Yuanye Biotechnology Co., Ltd (Shanghai, China). Sulfatase from *Helix pomatia* (S9626, containing sulfatase and β-glucuronidase) was obtained from Sigma-Aldrich (St. Louis, MO, USA).

2.2 Animals and drug administration

Eighteen male Sprague-Dawley rats (180-200 g) were obtained from Guangdong SijiaJingda Biological Technology Co., LTD (Guangzhou, China). The care of animals and all experimental procedures were approved by the Animal Ethics Committee of South China Agricultural University. Following a week of adaptive feeding, rats were randomized into two groups for plasma sample collection (n=10), and urine and feces sample collection (n=8). Rats in the HMF group received a single oral gavage of HMF (45 mg/kg) suspended in 0.5% CMC-Na, whereas the rats in the control group received an equal volume of 0.5% CMC-Na solution without HMF.

2.3 Sample collection

Prior to oral administration, ten rats (five in the control group and five in the HMF-treated group) were given free access to water and fasted overnight. Blood samples (about 0.4-0.5 mL) were collected periodically from the orbit at 0.5, 1, 2, 3, 4, 6, 8, 10, 24, 36 and 48 h after the oral administration (PO) of HMF. The plasma samples were obtained by centrifugation at 5000 rpm for 15 min and then stored at −80 °C until analysis. Eight rats, with four in the control group and four in the HMF-treated group, were housed individually in a metabolic cage to collect urine and feces sample. Urine and feces samples were collected during the following intervals: 0-12, 12-24, 24-36, and 36-48 hr after the first oral administration (a single-dose PO). After the 48 hr-collection, rats were orally administered by gavage daily from day 3 to day 7 to collect 24-hr urine and feces samples for analysis of the biotransformation process during consecutive intake of HMF (consecutive-dose PO).

2.4 Sample preparation

Plasma, urine and feces samples were prepared with and without enzymatic treatment according to previous studies with modifications[20, 25, 26]. Prior to sample extraction, plasma and urine were thawed and

then centrifuged at 5000 rpm for 10 min at 4 °C to obtain a clear supernatant. Two aliquots of plasma (100 μL each) and urine (50 μL each) samples were separately transferred to 2 mL tubes. One aliquot was extracted without enzymatic hydrolysis to detect metabolites in their native forms (both free forms and intact conjugates). This aliquot was directly subjected to protein precipitation using 800 μL of methanol-acetonitrile (50:50, v/v), enabling the concurrent extraction of both free and conjugated forms of HMF metabolites. The mixture was stirred in a vortex mixer for 5 min and then sonicated. After centrifugation at 14000 rpm for 15 min at 4 ℃, the supernatant was collected. Then the residue was extracted again with 800 μL of methanol-acetonitrile (50:50, v/v). The combined supernatants were evaporated to dryness using a Speed Vac concentrator. Finally, the dry residue was redissolved with 50% acetonitrile for UPLC-HRMS/MS Analysis.

To enable the identification and semi-quantitative analysis of all demethylated metabolites, the second aliquot was subjected to enzymatic hydrolysis by pre-incubation with a mixture of β-glucuronidase and sulfatase at 37 °C for 45 min, thereby cleaving glucuronide and sulfate conjugates to release the deconjugated forms for detection. After incubation, 800 μL of methanol-acetonitrile (50:50, v/v) was added to terminate the reaction, and the sample was extracted twice according to the aforementioned procedure. For feces samples, the collected samples were lyophilized and homogenized before sample preparation. Two aliquots of freeze-dried feces samples were weighed (5 mg each) and suspended in 100 μL of PBS buffer. Subsequently, the rest process of extraction and enzymatic treatment were identical to those for plasma and urine pretreatment.

2.5 UPLC-HRMS/MS analysis

The qualitative analysis was carried out on an UHPLC-LTQ-Orbitrap Velos mass spectrometer (Thermo Scientific, Bremen, Germany) equipped with an autosampler, a quaternary pump and a heated electrospray ionization (HESI) source. A poroshell 120 PFP column (4.6 ×150 mm, 2.7 μm, Agilent, Santa Clara, CA, USA) was used to effectively separate the isomeric metabolites. The mobile phase was composed of 0.1% formic acid in water (A) and 0.1% formic acid in acetonitrile (B) with a flow rate of 0.6 mL/min. The gradient elution program was as follows: 0–4 min, linear from 10% to 30% B; 4–20 min, linear from 30% to 60% B; 20–23 min, linear from 60% to 90% B; 23–25 min, 90% B; 25–25.5 min, linear from 90% to 10% B; 25.5–30 min, 10% B used to equilibrate the column. The temperature of the column remained at 30 °C and the injection volume was 20 μL. Mass spectrum acquisition was carried out in the positive ion mode through the HESI source. The parameters of HESI source and MS/MS conditions were optimized using the standard of HMF. The optimized ion source parameters were set as follows: probe heater temperature of 350 °C, capillary temperature of 380 °C, ISpray voltage of 4 kV, sheath gas flow of 60 arbitrary units, aux gas flow of 30 arbitrary units, S-lens levels of 65% and automatic gain control (AGC) of 1×10^5.

For metabolite identification, HRMS/MS was carried out by full scan/data-dependent secondary scan (full mass/dd-MS^2) mode. Data-dependent analysis (DDA) was triggered by the top 3 most intense ions, and the parent ion list (PIL)-DE dependent acquisition mode and then MS/MS scan mode were used as complementary method to improve the characterization of MS^2 spectrum. The mass resolutions were 30000

for full scan and 7500 for the MS/MS scans, and the scan range was *m/z* 100−1000. Higher-energy collisional dissociation (HCD) mode was employed to produce a larger number of product ions with a collision energy of 60 eV. Data acquisition and analysis were performed using Xcalibur 4.1 software (Thermo Fisher Scientific).

2.6 Semiquantitative analysis of all demethylated metabolites of HMF

Given the dynamic interconversion between free and conjugated forms of demethylated metabolites *in vivo*[16], it is essential to quantify their total abundance. Therefore, enzymatic hydrolysis was employed to convert conjugated forms of demethylated metabolites into their free forms[27], thereby allowing estimation of their total abundance.

To comprehensively characterize HMF's metabolic profile, we utilized a single full-scan MS mode on UHPLC-Q-Orbitrap HRMS for semiquantitative analysis. This approach was selected due to the lack of commercial standards for most metabolites and the need to simultaneously monitor multiple analytes. Prior studies have validated the use of full-scan HRMS for quantitating pharmaceuticals and endogenous metabolites in complex matrices[28, 29]. High-resolution extracted ion chromatograms (HREIC) were generated with a mass extraction window of 10 ppm around the theoretical *m/z* of each analyte for quantitation. Most free-form demethylated metabolites showed good peak shapes and separation in the HREIC, which were eligible for quantitative analysis. The relative quantitative estimation of all demethylated metabolites was performed to further investigate the biotransformation process of HMF in the serum, urine and feces by the area normalization method. This involved calculating the percentage of each analyte's peak area relative to the total peak area of all detected HMF-derived compounds.

3. Results

3.1 Analytical workflow for identification of HMF metabolites in vivo

On the basis of previous studies on the identification of flavonoids[30-32], an effective strategy for the systematic screening and identification metabolites of HMF was established using UHPLC-LTQ-Orbitrap HRMS/MS combined with enzymatic hydrolysis pretreatment and advanced data acquisition/processing techniques. The analytical workflow was divided into three steps (Figure 2). Citrus flavonoids undergo extensive phase I and II metabolisms *in vivo*[15]. However, the glucuronide and sulfate conjugates exhibit structural diversity due to abundant phenolic hydroxyl groups in their chemical architecture. These conjugates demonstrate poor ionization efficiency in positive ion mode, resulting in challenges for chromatographic separation and mass spectrometric detection[27, 33]. Therefore, in order to identify as many deconjugated metabolites as possible *in vivo*, samples were subjected to enzymatic hydrolysis with glucuronidase and sulfatase, in which the deconjugated metabolites were liberated from their conjugated forms and could be easily detected in the MS[27, 33]. To comprehensively capture both free and conjugated metabolites, each biological sample was processed in two parallel aliquots: one aliquot was extracted without enzymatic hydrolysis to preserve native metabolite forms (both free and conjugated forms), while the second aliquot was pretreated with β-glucuronidase and sulfatase to hydrolyze glucuronide and sulfate conjugates, thereby

releasing deconjugated metabolites for detection. Integration analysis of metabolic characterization in pre-treatment with and without enzymatic hydrolysis was used to systematically investigate the metabolite profiles of HMF (Step 1). In Step 2, data acquisition was performed on UHPLC-LTQ-Orbitrap MS^n in positive ion mode, in which accurate MS was obtained by full-scan data acquisition and MS^2 was obtained by data-dependent acquisition. Then, the characterization of potential metabolites, including secondary mass spectrometry information and isomers, could be further improved by PIL-including DDA and MS^2 scans, respectively. The cleavage pathways of HMF standard were analyzed by high-resolution MS/MS under HCD mode, and diagnostic product ions (DPIs) were identified for screening and structural identification of metabolites. In Step 3, HMF metabolites were identified according to the accurate mass data acquired, DPIs derived from HMF's fragmentation patterns and PMFs' biotransformation knowledge.

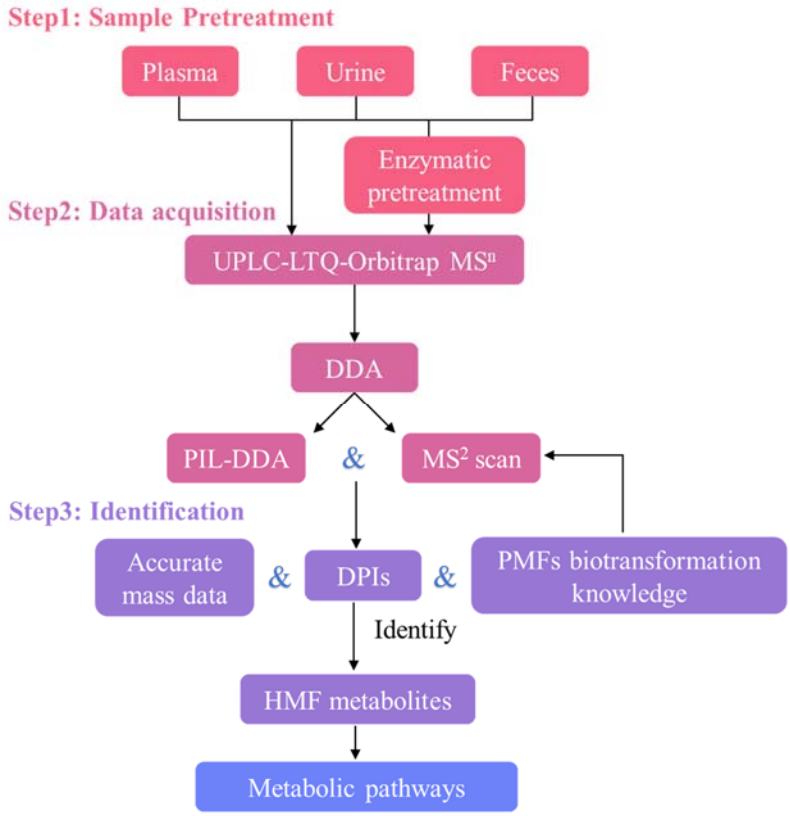

Figure 2. Analytical workflow for identification of HMF metabolites *in vivo*.

3.2 Optimization of fragmentation modes and collision energy in UHPLC-HRMS/MS

In order to obtain more fragmentation information for characterizing HMF, including its characteristic fragmentation pathways and DPIs, collision-induced dissociation (CID) and HCD and their collision energy were optimized. As shown in Figures 3A and 3E, the fragment richness was greater in HCD mode than in CID mode, with HCD mode generating abundant low-mass product ions below *m/z* 385, indicating that HCD mode could provide more extensive fragmentation beneficial for characterizing HMF structures. An increased fragment richness was observed using higher collision energy in HCD mode (Figure 3B-F). In this study, the optimal collision energy was found to be 60 eV, yielding ions at *m/z* 345.0605 and 403.1024 as the most abundant product ions, and characteristic product ions at *m/z* 165.0547, 178.0826, 183.0289 and 211.0238.

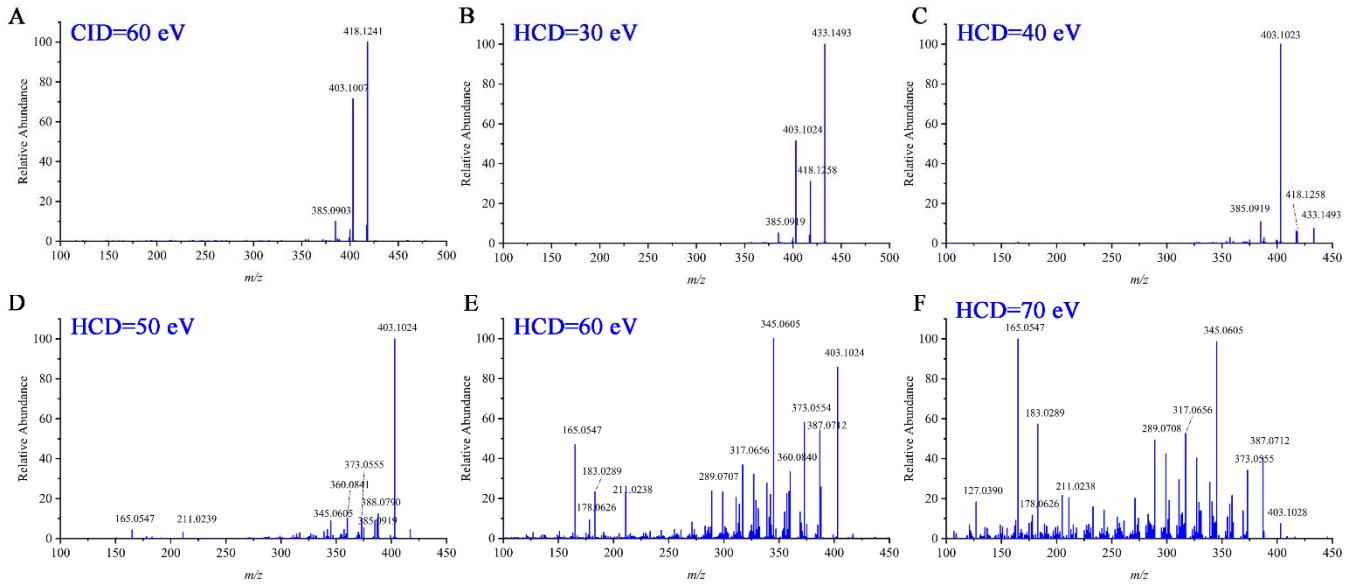

Figure 3. Optimization of fragmentation modes and collision energies using UHPLC-LTQ-Orbitrap HRMS/MS. The MS^2 spectra were acquired using CID at 60 eV (A) and HCD at collision energies from 30 to 70 eV (B-F).

3.3 Fragmentation pathways of HMF

Based on the similarity in mass fragmentations between parent compounds and their metabolites, it is important to analyze the fragmentation pathways of the parent compound[34]. Therefore, the mass spectrometric behaviors of HMF standard were investigated (Figure 4). Under positive HESI mode, HMF molecule ($C_{22}H_{24}O_9$) easily generated a protonated molecular ion of *m/z* 433.1494 (mass error 0.21 ppm) and was eluted at 16.16 min. In the MS^2 spectrum, three characteristic ions at *m/z* 403.1024, 373.0554, and 345.0605 were generated from HMF protonated by successively losing $2{\cdot}CH_3$, $2{\cdot}CH_3$ and CO, respectively. These finding correlated well with previous results where the protonated PMFs tend to loss radical ($\cdot CH_3$) or neutral molecules (CO)[35, 36]. Furthermore, the protonated HMF could undergo retro-Diels-Alder (RDA) cleavage in 0,2- or 1,3-position of the C-ring under the high collision energy in HCD mode (Figure 4D), forming four crucial fragment ions at *m/z* 165.0547 ($^{0,2}B^+$), 178.0826 ($^{1,3}B^+$), 183.0289 ($^{1,3}A^+$) and 211.0238 ($^{1,3}A^+$). These RDA ions indicated that there were four methoxy substituents at ring A, two at ring B and one at ring C. Hence, these four characteristic fragment ions arising from RDA reactions were regarded as DPIs, which could provide important information to identify the substituents of hydroxyl (OH) or methoxy (OMe) groups on the A, B and C rings of HMF metabolites[35, 36]. The predominant fragmentation pathways of HMF were proposed as shown in Figure 4C.

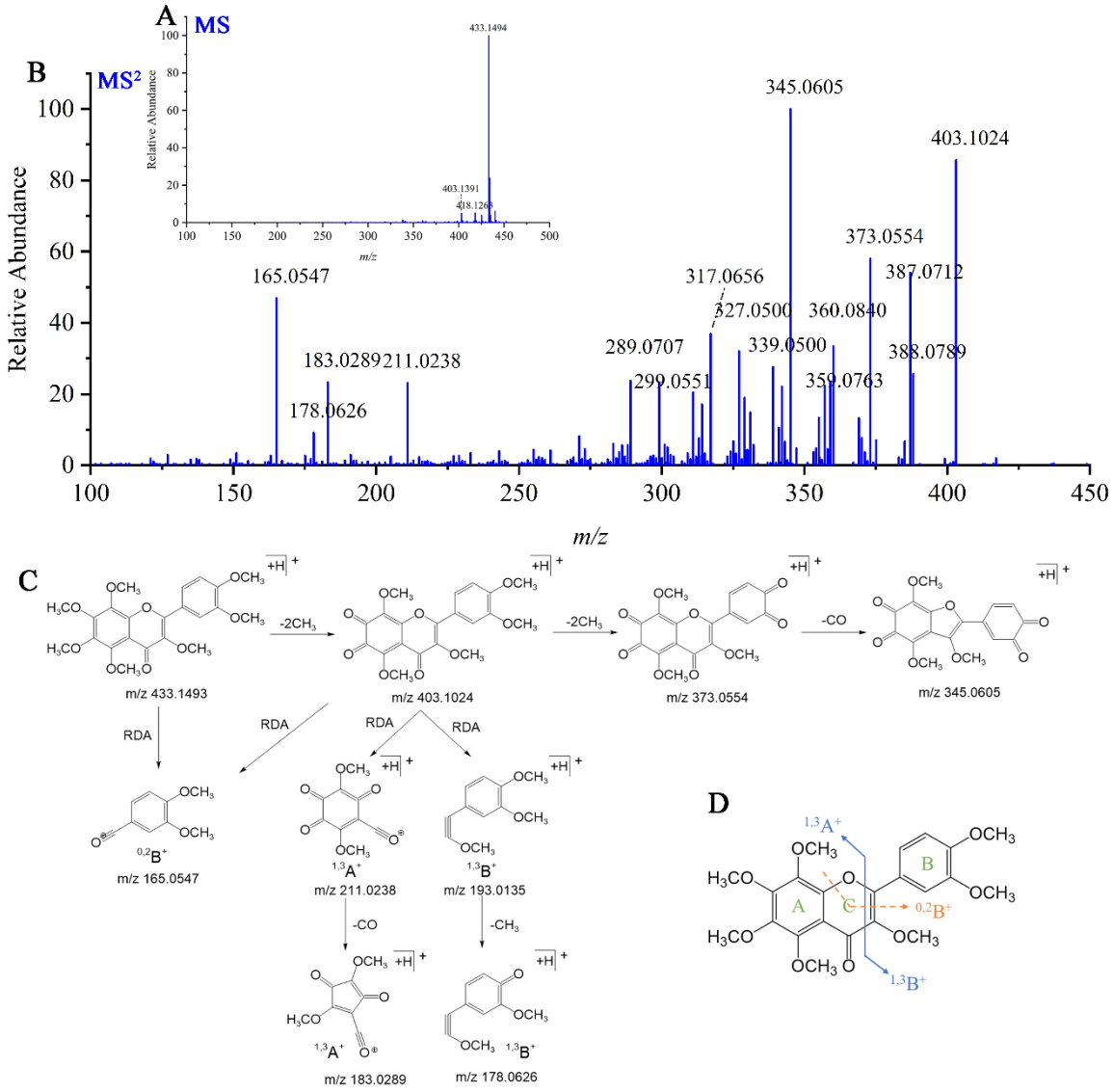

Figure 4. (A) MS and (B) MS^2 spectra of the HMF standard, and (C) the predominant fragmentation pathways of HMF. (D) Retro-Diels-Alder (RDA) cleavage pattern of HMF. MS data were acquired in positive ionization mode by FT full-scan. The MS^2 data were obtained from the precursor ion at *m/z* 433.14 using HCD at 60 eV collision energy.

3.4 Identification of HMF metabolites in vivo

In accordance with the analytical strategy described above, this study comprehensively investigated the *in vivo* metabolism of HMF. As summarized in Table 1, a total of 56 HMF metabolites were tentatively identified in rat plasma, urine and feces, including 37 demethylated metabolites and 19 their glucuronidation products. To facilitate structural elucidation and description, these metabolites were classified into eight groups based on their metabolic reactions: mono-demethylated (7), di-demethylated (13), tri-demethylated (9), tetra-demethylated (7), and penta-demethylated metabolites (1), as well as glucuronide conjugates of mono- (4), di- (6), and tri-demethylated metabolites (9). Furthermore, the distribution of hydroxyl or methoxy substituents on the A-, B-, and C-rings of the demethylated metabolites was inferred based on RDA cleavage patterns. The detailed metabolite information is shown in Table 1. Representative MS and MS^2 spectra of HMF metabolites, along with proposed fragmentation pathways for HMF metabolites, are included in the Supporting Information.

Table 1. Identification and characterization of HMF metabolites in rat urine, feces and plasma.[a]

NO	tR (min)	Identification	Formula	Measured mass $[M+H]^+$ (*m/z*)	Calculated mass $[M+H]^+$ (*m/z*)	Error (ppm)	MS^2 fragmentation	The distribution of substituents			Description[b]	Reaction	U	F	P
								Substituent in A ring	Substituent in B ring	Substituent in C ring					
M0	16.16	Heptamethoxyflavone	$C_{22}H_{24}O_9$	433.1491	433.14931	-0.48	403.1024, 345.0605, 373.0555,165.0547, 387.0713, 317.0656, 360.0841, 211.0240, 183.0290, 178.0629	$4OCH_3$	$2OCH_3$	OCH_3	HMF		+	+	+
M1-1	12.61	Monohydroxy-hexamethoxyflavone	$C_{21}H_{22}O9$	419.133	419.13366	-1.57	389.0863, 346.0683, 165.0545, 343.0443, 374.0632, 328.0576, 359.0396, 178.0623, 169.013, 197.0082	$3OCH_3$ + OH	$2OCH_3$	OCH_3	HMF-A1 (7-OH HMF)	mono-demethylation	+	+	+
M1-2	12.98	Monohydroxy-hexamethoxyflavone	$C_{21}H_{22}O_9$	419.1333	419.13366	-0.86	389.0865, 165.0546, 346.0681, 343.0446, 328.0577, 374.0633, 331.0446, 178.0625, 197.0079, 169.0129	$3OCH_3$ + OH	$2OCH_3$	OCH_3	HMF-A1 (6-OH HMF)	mono-demethylation	+	+	+
M1-3	13.16	Monohydroxy-hexamethoxyflavone	$C_{21}H_{22}O_9$	419.1331	419.13366	-1.34	389.0866, 346.0681, 328.0575, 165.0545, 371.0759, 331.0449, 343.0447, 197.0082, 178.0624, 169.0132	$3OCH_3$ + OH	$2OCH_3$	OCH_3	HMF-A1 (8-OH HMF)	mono-demethylation	+	+	+
M1-4	13.59	Monohydroxy-hexamethoxyflavone	$C_{21}H_{22}O_9$	419.1331	419.13366	-1.34	389.0864, 331.0447, 373.0551, 374.0631, 359.0394, 151.0388, 346.0683, 211.0236, 183.0285, 164.0468	$4OCH_3$	OCH_3+ OH	OCH_3	HMF-B1 (3'-OH HMF)	mono-demethylation	+	+	+
M1-5	13.94	Monohydroxy-hexamethoxyflavone	$C_{21}H_{22}O_9$	419.133	419.13366	-1.57	389.0864, 331.0448, 359.0398, 151.0389, 374.0627, 373.0551, 346.0685, 211.0236, 183.0288, 164.0466	$4OCH_3$	OCH_3+ OH	OCH_3	HMF-B1(4'-OH HMF)	mono-demethylation	+	+	+
M1-6	17.19	Monohydroxy-hexamethoxyflavone	$C_{21}H_{22}O_9$	419.1334	419.13366	-0.62	328.0578, 389.0865, 346.0683, 331.0449, 361.0918, 165.0546, 211.0235, 183.0287, 151.0749, 163.0393	$4OCH_3$	$2OCH_3$	OH	HMF-C1 (3-OH HMF)	mono-demethylation	+	+	+
M1-7	20.34	Monohydroxy-hexa	$C_{21}H_{22}$	419.13	419.13	-0.86	389.0865, 328.0576, 346.0683,	$3OCH_3$ +	$2OCH_3$	OCH_3	HMF-A1	mono-de	+	+	+

		methoxyflavone	O_9	33	366		165.0546, 331.0446, 361.0918, 371.0759, 197.0081, 178.0624, 169.0133	OH			(5-OH HMF)	methylation			
M2-1	10.39	Dihydroxy-pentamethoxyflavone	$C_{20}H_{20}O_9$	405.1177	405.11801	-0.77	375.0707, 332.0526, 360.0472, 347.0759, 151.0388, 317.0292, 314.0416, 164.0466, 169.0133, 197.0078	$3OCH_3$ + OH	OCH_3+ OH	OCH_3	HMF-A1B1	di-demethylation	+	+	+
M2-2	10.63	Dihydroxy-pentamethoxyflavone	$C_{20}H_{20}O_9$	405.1176	405.11801	-1.01	375.0708, 332.0525, 360.0471, 151.0388, 347.0758, 314.0418, 317.0290, 197.008, 169.0130, 164.0468	$3OCH_3$ + OH	OCH_3+ OH	OCH_3	HMF-A1B1	di-demethylation	+	+	+
M2-3	10.86	Dihydroxy-pentamethoxyflavone	$C_{20}H_{20}O_9$	405.1178	405.11801	-0.52	375.0708, 151.0388, 332.0526, 360.0475, 314.0418, 197.0080, 357.0601, 317.0287, 164.0468, 169.0129	$3OCH_3$ + OH	OCH_3+ OH	OCH_3	HMF-A1B1	di-demethylation	+	+	+
M2-4	11.13	Dihydroxy-pentamethoxyflavone	$C_{20}H_{20}O_9$	405.1178	405.11801	-0.52	375.0707, 332.0525, 357.0602, 151.0388, 360.0475, 314.0420, 356.0522, 197.0078, 164.0467, 169.0131	$3OCH_3$ + OH	OCH_3+ OH	OCH_3	HMF-A1B1	di-demethylation	+	+	+
M2-5	11.31	Dihydroxy-pentamethoxyflavone	$C_{20}H_{20}O_9$	405.1175	405.11801	-1.26	375.0710, 332.0527, 314.0419, 151.0389, 357.0604, 360.0475, 329.0653, 197.0079, 164.0469, 169.0131	$3OCH_3$ + OH	OCH_3+ OH	OCH_3	HMF-A1B1	di-demethylation	+	+	+
M2-6	11.65	Dihydroxy-pentamethoxyflavone	$C_{20}H_{20}O_9$	405.1178	405.11801	-0.52	375.0707, 359.0396, 317.0288, 332.0527, 137.0232, 360.0472, 211.0235, 314.0419, 183.0283, 150.0311	$4OCH_3$	2OH	OCH_3	HMF-B2 (3',4'-diOH HMF)	di-demethylation	+	+	+
M2-7	14.57	Dihydroxy-pentamethoxyflavone	$C_{20}H_{20}O_9$	405.1177	405.11801	-0.77	332.0511, 314.0408, 375.0694, 347.0745, 317.0276, 329.0642, 151.0384, 183.0279, 211.0228, 137.0594	$4OCH_3$	OCH_3+ OH	OH	HMF-B1C1	di-demethylation	+	+	-
M2-8	14.89	Dihydroxy-pentamethoxyflavone	$C_{20}H_{20}O_9$	405.1177	405.11801	-0.77	314.0409, 332.0514, 375.0696, 347.0746, 317.0278, 151.0385, 329.0644, 211.0231, 137.0592, 183.0283	$4OCH_3$	OCH_3+ OH	OH	HMF-B1C1	di-demethylation	+	+	-
M2-9	15.96	Dihydroxy-pentamethoxyflavone	$C_{20}H_{20}O_9$	405.1179	405.11801	-0.27	375.0709, 332.0525, 360.0475, 151.0389, 347.0761, 317.029, 314.0420, 169.0132, 197.0080, 164.0468	$3OCH_3$ + OH	OCH_3+ OH	OCH_3	HMF-A1B1	di-demethylation	+	+	+
M2-1	16.68	Dihydroxy-pentame	$C_{20}H_{20}$	405.11	405.11	-0.77	332.0525, 375.0708, 347.0757,	$2OCH_3$ +	$2OCH_3$	OCH_3	HMF-A2	di-demet	+	+	+

0		thoxyflavone	O_9	77	801		317.0291, 329.0653, 165.0545, 304.0576, 178.0623, 182.9922, 154.9973	OH				hylation			
M2-11	17.44	Dihydroxy-pentamethoxyflavone	$C_{20}H_{20}O_9$	405.1179	405.11801	-0.27	332.0534, 347.0769, 329.0664, 317.0299, 375.0721, 357.0615, 389.0875, 165.0551, 178.0630, 182.9927	$2OCH_3$ + OH	$2OCH_3$	OCH_3	HMF-A2	di-demethylation	+	+	+
M2-12	17.81	Dihydroxy-pentamethoxyflavone	$C_{20}H_{20}O_9$	405.1177	405.11801	-0.77	375.0709, 332.0526, 314.0419, 347.0760, 357.0603, 360.0474, 151.0390, 197.0080, 164.0466, 169.0130	$3OCH_3$ + OH	OCH_3+ OH	OCH_3	HMF-A1B1	di-demethylation	+	+	-
M2-13	18.27	Dihydroxy-pentamethoxyflavone	$C_{20}H_{20}O_9$	405.1177	405.11801	-0.77	375.0710, 314.0421, 332.0526, 151.0389, 347.0761, 360.0475, 357.0601, 197.0080, 164.0470, 169.0132	$3OCH_3$ + OH	OCH_3+ OH	OCH_3	HMF-A1B1	di-demethylation	+	+	-
M3-1	8.62	Trihydroxy-tetramethoxyflavone	$C_{19}H_{18}O_9$	391.1024	391.10236	0.10	361.0549, 318.0366, 151.0388, 346.0314, 290.0417, 333.0600, 164.0465, 315.0496, 201.0029, 182.9921	$2OCH_3$ + 2OH	OCH_3+ OH	OCH_3	HMF-A2B1	tri-demethylation	+	+	-
M3-2	8.83	Trihydroxy-tetramethoxyflavone	$C_{19}H_{18}O_9$	391.1023	391.10236	-0.15	361.0551, 318.0367, 333.0603, 137.0231, 346.0314, 315.0497, 343.0446, 169.0130, 197.0080, 150.0310	$3OCH_3$ + OH	2OH	OCH_3	HMF-A1B2	tri-demethylation	+	+	+
M3-3	9.02	Trihydroxy-tetramethoxyflavone	$C_{19}H_{18}O_9$	391.1024	391.10236	0.10	361.0551, 318.0367, 137.0232, 346.0316, 197.0080, 343.0446, 300.0262, 215.0186, 150.0311, 169.0131	$3OCH_3$ + OH	2OH	OCH_3	HMF-A1B2	tri-demethylation	+	+	-
M3-4	9.48	Trihydroxy-tetramethoxyflavone	$C_{19}H_{18}O_9$	391.1022	391.10236	-0.41	361.0551, 318.0366, 343.0446, 137.0232, 300.0262, 346.0317, 197.0079, 315.0498, 150.0309, 169.0128	$3OCH_3$ + OH	2OH	OCH_3	HMF-A1B2	tri-demethylation	+	+	+
M3-5	12.40	Trihydroxy-tetramethoxyflavone	$C_{19}H_{18}O_9$	391.1022	391.10236	-0.41	318.0367, 333.0604, 361.0552, 300.0262, 315.0498, 137.0232, 346.0316, 272.0312, 123.0444, 211.0223	$4OCH_3$	2OH	OH	HMF-B2C1 (3,3',4'-TriOH HMF)	tri-demethylation	+	+	+
M3-6	13.66	Trihydroxy-tetramethoxyflavone	$C_{19}H_{18}O_9$	391.1013	391.10236	-2.71	333.0597, 318.0361, 361.0545, 151.0387, 343.0438, 290.0415, 315.0493, 164.0464, 182.9922, 154.9977	$2OCH_3$ + 2OH	OCH_3+ OH	OCH_3	HMF-A2B1	tri-demethylation	+	+	-
M3-7	14.17	Trihydroxy-tetramet	$C_{19}H_{18}$	391.10	391.10	-0.66	361.0555, 318.0370, 333.0608,	$2OCH_3$ +	OCH_3+	OCH_3	HMF-A2B1	tri-demet	+	+	-

		hoxyflavone	O_9	21	236		315.0502, 346.0321, 151.0390, 303.0137, 164.0468, 182.9927, 154.9975	2OH	OH			hylation			
M3-8	14.55	Trihydroxy-tetramethoxyflavone	$C_{19}H_{18}O_9$	391.1013	391.10236	-2.71	361.0555, 318.0371, 333.0608, 315.0501, 346.0320, 151.0391, 290.0423, 343.0449, 164.0470, 182.9928	$2OCH_3$ + 2OH	OCH_3+ OH	OCH_3	HMF-A2B1	tri-demethylation	+	+	-
M3-9	15.65	Trihydroxy-tetramethoxyflavone	$C_{19}H_{18}O_9$	391.1021	391.10236	-0.66	361.0553, 318.0370, 333.0606, 300.0264, 343.0446, 137.0233, 346.0319, 197.0081, 169.0132, 150.0312	$3OCH_3$ + OH	2OH	OCH_3	HMF-A1B2	tri-demethylation	+	+	+
M4-1	7.40	Tetrahydroxy-trimethoxyflavone	$C_{18}H_{16}O_9$	377.0861	377.08671	-1.62	347.0394, 304.0209, 137.0231, 348.0429, 319.0439, 150.0309, 182.9925, 332.0163, 201.0024, 154.9969	$2OCH_3$ + 2OH	2OH	OCH_3	HMF-A2B2	tetra-demethylation	+	+	-
M4-2	7.62	Tetrahydroxy-trimethoxyflavone	$C_{18}H_{16}O_9$	377.0861	377.08671	-1.62	347.0394, 301.0341, 304.0211, 137.0231, 319.0445, 348.0435, 361.0556, 150.0309, 182.9920, 154.9975	$2OCH_3$ + 2OH	2OH	OCH_3	HMF-A2B2	tetra-demethylation	+	+	-
M4-3	9.59	Tetrahydroxy-trimethoxyflavone	$C_{18}H_{16}O_9$	377.0862	377.08671	-1.35	319.0446, 304.0213, 347.0398, 329.0292, 276.0266, 245.0447, 137.0233, 197.0086, 169.0132, 123.0446	$3OCH_3$ + OH	2OH	OH	HMF-A1B2C1	tetra-demethylation	+	+	-
M4-4	9.72	Tetrahydroxy-trimethoxyflavone	$C_{18}H_{16}O_9$	377.0862	377.08671	-1.35	319.0443, 347.0395, 304.0209, 301.0340, 329.0284, 320.0471, 137.0231, 169.0134, 123.0440, 197.0097	$3OCH_3$ + OH	2OH	OH	HMF-A1B2C1	tetra-demethylation	+	+	-
M4-5	11.34	Tetrahydroxy-trimethoxyflavone	$C_{18}H_{16}O_9$	377.0862	377.08671	-1.35	319.0443, 347.0392, 304.0211, 346.0619, 137.0228, 320.0477, 329.0289, 276.0255, 150.0307, 182.9922	$2OCH_3$ + 2OH	2OH	OCH_3	HMF-A2B2	tetra-demethylation	+	+	-
M4-6	12.20	Tetrahydroxy-trimethoxyflavone	$C_{18}H_{16}O_9$	377.0862	377.08671	-1.35	347.0394, 304.0211, 319.0443, 301.034, 137.0232, 348.0426, 329.0282, 182.9923, 150.0312, 154.9969	$2OCH_3$ + 2OH	2OH	OCH_3	HMF-A2B2	tetra-demethylation	+	+	-
M4-7	14.58	Tetrahydroxy-trimethoxyflavone	$C_{18}H_{16}O_9$	377.0862	377.08671	-1.35	319.0444, 304.0211, 329.0288, 347.0398, 301.0342, 320.0477, 276.0259, 137.0232, 169.0131, 197.0078	$3OCH_3$ + OH	2OH	OH	HMF-A1B2C1	tetra-demethylation	+	+	-
M5	9.10	Pentahydroxy-dimet	$C_{17}H_{14}$	363.07	363.07	-1.54	305.0289, 347.0397, 333.0236,	OCH_3 +	2OH	OCH_3	HMF-A3B2	penta-de	+	+	-

		hoxyflavone	O_9	05	106		313.0337, 231.0286, 137.0233, 169.013, 147.0436, 123.0439,150.0316	3OH				methylation			
M6-1	8.55	Glucuronide conjugate of monohydroxy-hexamethoxyflavone	$C_{27}H_{30}O_{16}$	595.165	595.16575	-1.26	389.0866, 371.0760, 346.0685, 374.0631, 328.0579, 343.0811, 165.0547, 197.0084, 178.0627, 169.0142	$3OCH_3$ + OH	$2OCH_3$	OCH_3	HMF-A1+GluA	mono-demethylation + glucuronidation	+	+	+
M6-2	9.13	Glucuronide conjugate of monohydroxy-hexamethoxyflavone	$C_{27}H_{30}O_{16}$	595.1668	595.16575	1.76	389.0860, 346.0681, 374.0629, 371.0755, 361.0919, 343.0779, 343.0477, 165.0544, 197.0085, 169.0134	$3OCH_3$ + OH	$2OCH_3$	OCH_3	HMF-A1+GluA	mono-demethylation + glucuronidation	+	+	+
M6-3	9.54	Glucuronide conjugate of monohydroxy-hexamethoxyflavone	$C_{27}H_{30}O_{16}$	595.1649	595.16575	-1.43	389.0864, 331.0446, 373.0551, 359.0397, 151.0388, 374.0633, 346.0684, 183.0288, 211.0236, 164.0467	$4OCH_3$	OCH_3+ OH	OCH_3	HMF-B1+GluA	mono-demethylation + glucuronidation	+	+	+
M6-4	9.73	Glucuronide conjugate of monohydroxy-hexamethoxyflavone	$C_{27}H_{30}O_{16}$	595.1667	595.16575	1.60	165.0546, 389.0865, 328.0578, 331.0447, 346.0684, 343.0447, 197.008, 303.0498, 169.0132, 178.0626	$3OCH_3$ + OH	$2OCH_3$	OCH_3	HMF-A1+GluA	mono-demethylation + glucuronidation	+	+	+
M7-1	7.74	Glucuronide conjugate of dihydroxy-pentamethoxyflavone	$C_{26}H_{28}O_{15}$	581.149	581.1501	-1.89	375.0708, 151.0388, 317.0290, 332.0526, 360.0474, 314.0417, 347.0754, 169.0130, 164.0465, 197.0080	$3OCH_3$ + OH	OCH_3+ OH	OCH_3	HMF-A1B1+GluA	di-demethylation + glucuronidation	+	-	+
M7-2	7.96	Glucuronide conjugate of dihydroxy-pentamethoxyflavone	$C_{26}H_{28}O_{15}$	581.149	581.1501	-1.89	375.0708, 151.0388, 317.0290, 332.0526, 360.0474, 314.0417, 347.0754, 169.0130, 164.0465, 197.0080	$3OCH_3$ + OH	OCH_3+ OH	OCH_3	HMF-A1B1+GluA	di-demethylation + glucuronidation	+	+	-
M7-3	8.25	Glucuronide conjugate of dihydroxy-pentamethoxyflavone	$C_{26}H_{28}O_{15}$	581.149	581.1501	-1.89	375.0710, 151.039, 332.0527, 314.0422, 360.0475, 317.0292, 357.0602, 197.0078, 164.0469, 169.0133	$3OCH_3$ + OH	OCH_3+ OH	OCH_3	HMF-A1B1+GluA	di-demethylation + glucuronidation	+	+	+
M7-4	9.49	Glucuronide conjugate of	$C_{26}H_{28}O_{15}$	581.1492	581.1501	-1.55	375.0709, 359.0398, 317.0291, 137.0232, 332.0529, 331.0449,	$4OCH_3$	2OH	OCH_3	HMF-B2+GluA	di-demethylation	+	+	+

		dihydroxy-pentamethoxyflavone					183.0286, 360.0473, 211.0236, 150.0312					+ glucuronidation			
M7-5	9.85	Glucuronide conjugate of dihydroxy-pentamethoxyflavone	$C_{26}H_{28}O_{15}$	581.1492	581.1501	-1.55	314.0418, 332.0526, 347.0758, 317.0292, 375.0707, 289.0342, 299.0187, 151.0388, 329.0652, 286.0469	$3OCH_3$ + OH	OCH_3+ OH	OCH_3	HMF-A1B1 +GluA	di-demethylation + glucuronidation	+	+	-
M7-6	11.81	Glucuronide conjugate of dihydroxy-pentamethoxyflavone	$C_{26}H_{28}O_{15}$	581.1493	581.1501	-1.38	375.0709, 151.0388, 332.0527, 314.0420, 360.0472, 317.0291, 197.0081, 289.0338, 169.0131, 164.0468	$3OCH_3$ + OH	OCH_3+ OH	OCH_3	HMF-A1B1 +GluA	di-demethylation + glucuronidation	+	+	-
M8-1	7.28	Glucuronide conjugate of trihydroxy-tetramethoxyflavone	$C_{25}H_{26}O_{15}$	567.1341	567.13445	-0.62	361.0554, 137.0233, 318.0370, 197.0081, 346.0320, 300.0265, 343.0450, 215.0187, 169.0131, 150.0312	$3OCH_3$ + OH	2OH	OCH_3	HMF-A1B2 +GluA	tri-demethylation + glucuronidation	+	-	+
M8-2	7.42	Glucuronide conjugate of trihydroxy-tetramethoxyflavone	$C_{25}H_{26}O_{15}$	567.1335	567.13445	-1.68	361.0550, 318.0366, 137.0231, 333.0605, 300.0262, 346.0317, 345.0235, 169.0129, 197.0075, 150.0313	$3OCH_3$ + OH	2OH	OCH_3	HMF-A1B2 +GluA	tri-demethylation + glucuronidation	+	-	-
M8-3	7.70	Glucuronide conjugate of trihydroxy-tetramethoxyflavone	$C_{25}H_{26}O_{15}$	567.1337	567.13445	-1.32	361.0551, 318.0368, 333.0603, 137.0232, 300.0262, 346.0316, 329.0290, 169.0130, 197.0081, 150.0311	$3OCH_3$ + OH	2OH	OCH_3	HMF-A1B2 +GluA	tri-demethylation + glucuronidation	+	-	+
M8-4	8.09	Glucuronide conjugate of trihydroxy-tetramethoxyflavone	$C_{25}H_{26}O_{15}$	567.1337	567.13445	-1.32	361.0552, 318.0368, 137.0233, 343.0447, 300.0262, 197.0081, 346.0317, 315.0504, 150.0311, 169.0130	$3OCH_3$ + OH	2OH	OCH_3	HMF-A1B2 +GluA	tri-demethylation + glucuronidation	+	-	+
M8-5	8.22	Glucuronide conjugate of trihydroxy-tetramethoxyflavone	$C_{25}H_{26}O_{15}$	567.1345	567.13445	0.09	361.0553, 318.0368, 137.0233, 343.0447, 300.0265, 346.0316, 197.0077, 315.0495, 169.0133, 150.0310	$3OCH_3$ + OH	2OH	OCH_3	HMF-A1B2 +GluA	tri-demethylation + glucuronidation	+	-	-
M8-6	9.57	Glucuronide conjugate of	$C_{25}H_{26}O_{15}$	567.1328	567.13445	-2.91	361.0551, 318.0369, 333.0605, 303.0133, 315.0496, 151.0390,	$2OCH_3$ + 2OH	OCH_3+ OH	OCH_3	HMF-A2B1 +GluA	tri-demethylation	+	-	-

		trihydroxy-tetramethoxyflavone					346.0319, 164.0466, 182.9920, 154.9976					+ glucuronidation			
M8-7	9.81	Glucuronide conjugate of trihydroxy-tetramethoxyflavone	$C_{25}H_{26}O_{15}$	567.134	567.13445	-0.79	318.0367, 300.0263, 361.0552, 333.0605, 137.0232, 315.05, 272.0314, 275.0186, 303.0136, 290.0418	$3OCH_3$ + OH	2OH	OCH_3	HMF-A1B2 +GluA	tri-demethylation + glucuronidation	+	-	-
M8-8	11.88	Glucuronide conjugate of trihydroxy-tetramethoxyflavone	$C_{25}H_{26}O_{15}$	567.1336	567.13445	-1.50	361.0554, 318.0370, 300.0264, 333.0608, 137.0233, 343.0448, 346.0318, 197.0082, 150.0311, 169.0133	$3OCH_3$ + OH	2OH	OCH_3	HMF-A1B2 +GluA	tri-demethylation + glucuronidation	+	-	-
M8-9	12.15	Glucuronide conjugate of trihydroxy-tetramethoxyflavone	$C_{25}H_{26}O_{15}$	567.1345	567.13445	0.09	361.0549, 318.0367, 300.0261, 137.0232, 333.0602, 343.0445, 346.0317, 197.0080, 169.0129, 150.0311	$3OCH_3$ + OH	2OH	OCH_3	HMF-A1B2 +GluA	tri-demethylation + glucuronidation	+	-	-

Note:

[a]In the absence of authentic standards, the structures of HMF metabolites were tentatively identified based on the number and positions of demethylation.

[b]In metabolite description, A, B, and C denote the three aromatic rings of HMF, and the accompanying digit indicates the number of demethylations on that ring. GluA is the abbreviation for glucuronic acid.

Abbreviations: +, detected; –, not detected; U, urine; F, feces; P, plasma.

3.4.1 Monohydroxy-hexamethoxyflavone (M1)

Metabolites M1-1 to M1-7 were eluted at 12.61, 12.98, 13.16, 13.59, 13.94, 17.19 and 20.34 min, respectively, and all gave rise to protonated molecular ions at *m/z* 419.1330, 419.1333, 419.1331, 419.1331, 419.1330, 419.1334, and 419.1333 ($C_{21}H_{22}O_9$, mass error <1.26 ppm), respectively. Their protonated $[M+H]^+$ ions were 14 Da (CH_2) lower than HMF, suggesting that they were a group of isomers deduced as mono-demethylated metabolites of HMF. In the MS^2 spectra, they showed the same characteristic fragment product ions at *m/z* 389.0863, 359.0396 and 331.0446, which were generated after continuously losing $2\cdot CH_3$, $2\cdot CH_3$ and CO from protonated molecular ion (Figure S3-S4). In addition, they generated several DPIs after the RDA reaction, but these DPIs varied among the isomers and served to differentiate their structures (Figure S3). The MS^2 spectra of M1-1, M1-2, M1-3, and M1-7 displayed DPIs at *m/z* 165.0545 ($^{0,2}B^+$), 178.0624 ($^{1,3}B^+$), 169.0132 ($^{1,3}A^+$, 183.0289-CH_2), 197.0082 ($^{1,3}A^+$, 211.0238-CH_2). Notably, the two $^{1,3}A^+$ DPIs were 14 Da lower than their counterparts in M0, whereas the $^{0,2}B^+$ and $^{1,3}B^+$ DPIs remained unchanged, indicating that mono-demethylation occurred specifically on the A-ring. Consequently, these metabolites were tentatively identified as A-ring mono-demethylated metabolites (HMF-A1). Because there were four methoxy groups in the A ring of HMF, mono-demethylation could occur at the C-5, C-6, C-7, and C-8 positions of HMF. To distinguish these four A-ring mono-demethylated metabolites, their retention times in the reversed-phase (RP) chromatographic system were compared, revealing the elution order: M1-1 < M1-2 < M1-3 < M1-7. This order reflected increasing hydrophobicity, as compounds with higher hydrophobicity are retained longer under these conditions. As reported, the six monodemethylnobiletin isomers eluted on a RP column in the following order: 7- < 6- < 8- < 3′- < 4′- < 5-demethylnobiletin[37]. This order reflects a corresponding polarity trend for monohydroxy PMFs: 7-OH PMFs > 6-OH PMFs > 8-OH PMFs > 3′-OH PMFs > 4′-OH PMFs > 5-OH PMFs. Consequently, based on their relative polarities (reflected in elution order), M1-1, M1-2, M1-3, and M1-7 were tentatively identified as 7-OH HMF, 6-OH HMF, 8-OH HMF, and 5-OH HMF, respectively. Conversely, isomers M1-4 and M1-5 had the same DPIs at *m/z* 211.0236 ($^{1,3}A^+$) and 183.0288 ($^{1,3}A^+$) as M0, whereas their RDA fragmentation ions at *m/z* 151.0389 ($^{0,2}B^+$, 165.0547-CH_2) and 164.0466 ($^{1,3}B^+$, 178.0826-CH_2) in the B ring were 14 Da lower than the corresponding product ions of M0, suggesting that the mono-demethylation occurred at C-3′ or C-4′ position of B ring. According to the literature, 3′-OH PMFs showed shorter relative retention time in RP column compared to 4′-OH PMFs[25, 37, 38], and 4′-position were the major biotransformation sites[16]. Therefore, M1-4 and M1-5 were tentatively identified as 3′-OH HMF and 4′-OH HMF (HMF-B1), respectively. For metabolites M1-6, its DPIs were consistent with those of M0, suggesting that mono-demethylation occurred neither on the A- nor B- ring, but rather at the C-3 position of the C-ring. Thus, M1-6 was identified as 3-OH HMF. To our knowledge, this study represents the first simultaneous detection and structural discrimination of all seven mono-demethylated metabolites of HMF *in vivo*.

3.4.2 Dihydroxy-pentamethoxyflavone (M2)

A total of thirteen isomeric metabolites (M2-1 to M2-13) were detected, all with the molecular formula $C_{20}H_{20}O_9$ and $[M+H]^+$ ions at *m/z* 405.1175–405.1179 (mass error <1.26 ppm). The observed mass decrease of 28 Da (equivalent to the loss of two methyl groups) from the parent HMF confirmed their identities as di-demethylated metabolites. According to DPIs produced by the RDA cleavage, these metabolites were categorized into four distinct structural types. For the first type (HMF-A1B1), M2-1, M2-2, M2-3, M2-4, M2-5, M2-9, M2-12 and M2-13 displayed DPIs at *m/z* 169.0133 ($^{1,3}A^+$, 183.0289-CH_2), 197.0078 ($^{1,3}A^+$, 211.0238-CH_2), 151.0388 ($^{0,2}B^+$, 165.0547-CH_2), and 164.0466 ($^{1,3}B^+$, 178.0826-CH_2) in the MS^2 spectra. All these DPIs were 14 Da lower than their M0 counterparts, indicating that one demethylation had occurred on the A-ring and another on the B-ring. Thus, they were preliminarily identified as A-ring and B-ring mono-demethylated metabolites (HMF-A1B1). For the second type (HMF-A2), metabolites M2-10 and M2-11 showed A-ring DPIs at *m/z* 154.9973 ($^{1,3}A^+$, 183.0289-C_2H_4) and 182.9922 ($^{1,3}A^+$, 211.0238-C_2H_4), which were 28 Da lower than those of M0, while the B-ring DPIs remained unchanged. This suggested the loss of two methyl groups specifically from the A-ring, thus identifying them as A-ring di-demethylated metabolites. For the third type (HMF-B2), metabolite M2-6 exhibited B-ring DPIs at *m/z* 137.0232 and 150.0311, which were 28 Da lower than those in M0, while the A-ring DPIs remained unchanged. This suggested the loss of two methyl groups from the B-ring, specifically at the C-3′ and C-4′ positions, identifying it as 3′,4′-dihydroxy-3,5,6,7,8-pentamethoxyflavone. The last type of M2 metabolites (HMF-B1C1) yielded the same DPIs at *m/z* 151.0384 ($^{0,2}B^+$), 137.0594 ($^{1,3}B^+$), 183.0279 ($^{1,3}A^+$), 211.0228 ($^{1,3}A^+$), which indicated that one methyl loss occurred on the B-ring and the other on the C-ring (C-3 position). Therefore, M2-7 and M2-8 were tentatively identified as B-ring and C-ring mono-demethylated metabolites.

3.4.3 Trihydroxy-tetramethoxyflavone (M3)

Nine isomeric metabolites (M3-1 to M3-9) were identified, yielding protonated molecular ions at *m/z* 391.1024, 391.1023, 391.1024, 391.1022, 391.1022, 391.1013, 391.1021, 391.1013 and 391.1021(mass error <2.71 ppm), respectively. The mass weight was 42 Da (C_3H_6) lower more than that of M0, thereby identifying them as tri-demethylated metabolites of HMF. Similarly, these metabolites were classified into three structural types on the basis of DPIs. For the first type (HMF-A2B1), metabolites M3-1, M3-6, M3-7, and M3-8 were tentatively identified as A-ring di-demethylated and B-ring mono-demethylated metabolites of HMF. Their identification was based on DPIs indicative of di-demethylation on the A-ring (*m/z* 154.9977 ($^{1,3}A^+$, 183.0289-C_2H_4) and 182.9921 ($^{1,3}A^+$, 211.0238-C_2H_4)) and mono-demethylation on the B-ring (*m/z* 151.0388 ($^{0,2}B^+$, 165.0547-CH_2) and 164.0465 ($^{1,3}B^+$, 178.0826-CH_2)). For the second type (HMF-A1B2), metabolites M3-2, M3-3, M3-4, and M3-9 were characterized as A-ring mono-demethylated and B-ring di-demethylated metabolites of HMF. Their MS^2 spectra revealed DPIs for A-ring mono-demethylation at *m/z* 169.0130 ($^{1,3}A^+$, 183.0289-CH_2) and 197.0080 ($^{1,3}A^+$, 211.0238-CH_2), and for B-ring di-demethylation at *m/z* 137.0231 ($^{0,2}B^+$, 165.0547-C_2H_4) and150.0310 ($^{1,3}B^+$, 178.0826-C_2H_4). For the third type (HMF-B2C1), metabolite M3-5 was identified as a B-ring di-demethylated and C-ring mono-demethylated metabolite. The structure was deduced

from the presence of B-ring DPIs at *m/z* 137.0232 ($^{0,2}B^+$) and 123.0444 ($^{1,3}B^+$), alongside an unchanged A-ring DPI at *m/z* 211.0223 ($^{1,3}A^+$). With the A-ring intact and two demethylations assigned to the B-ring, the third demethylation must therefore be localized to the C-ring. Thus, M3-5 was determined to be 3′,4′,3-trihydroxy-5,6,7,8-tetramethoxyflavone.

3.4.4 Tetrahydroxy-trimethoxyflavone (M4)

Seven isomeric metabolites (M4-1 to M4-7) showed protonated molecular ions $[M+H]^+$ at *m/z* 377.0861-377.0862 ($C_{18}H_{16}O_9$, mass error <1.62 ppm). These metabolites were 56 Da (C_4H_8) lower than that of M0, indicating that they might be tetra-demethylated metabolites of HMF. Based on their DPIs, these metabolites were categorized into two structural types. The first type, comprising M4-1, M4-2, M4-5, and M4-6, was characterized as A-ring and B-ring di-demethylated metabolites (HMF-A2B2). Their MS^2 spectra exhibited a consistent set of DPIs at *m/z*137.0231 ($^{0,2}B^+$, 165.0547-C_2H_4), 150.0309 ($^{1,3}B^+$, 178.0826-C_2H_4), 154.9969 ($^{1,3}A^+$, 183.0289-C_2H_4) and 182.9925 ($^{1,3}A^+$, 211.0238-C_2H_4). These DPIs were 28 Da lower than their counterparts in M0, confirming the loss of two methyl groups from both the A- and B-rings. The second type, including M4-3, M4-4, and M4-7, was identified as A-ring mono-demethylated and B-ring di-demethylated metabolites, with an additional demethylation on the C-ring (HMF-A1B2C1). The structure was deduced from the presence of B-ring DPIs at *m/z* 137.0233 ($^{0,2}B^+$, 165.0547-C_2H_4) and 123.0446 ($^{1,3}B^+$), alongside two A-ring DPIs at *m/z* 169.0132 ($^{1,3}A^+$, 183.0289-CH_2) and 197.0086 ($^{1,3}A^+$, 211.0238-CH_2).

3.4.5 Pentahydroxy-dimethoxyflavone (M5)

Metabolite M5 was observed at 9.10 min with a protonated molecular ion at *m/z* 363.0705 ($C_{17}H_{14}O_9$, mass error 1.54 ppm). This mass was 70 Da (C_5H_{10}) lower than that of M0, identifying M5 as a penta-demethylated metabolite of HMF. Its structure was characterized as an A-ring tri-demethylated and B-ring di-demethylated metabolite (HMF-A3B2) based on its DPIs. Key B-ring DPIs at *m/z* 137.0233 ($^{0,2}B^+$, 165.0547-C_2H_4) and150.0316 ($^{1,3}B^+$, 178.0826-C_2H_4) confirmed the loss of two methyl groups from the B-ring, while two A-ring DPIs ions at *m/z* 183.9996 ($^{1,3}A^+$) and 169.013 ($^{1,3}A^+$) indicated the loss of three methyl groups from the A-ring, collectively supporting the proposed structure.

3.4.6 Glucuronide conjugates of monohydroxy-hexamethoxyflavone (M6)

Four isomeric metabolites (M6-1 to M6-4) were eluted at 8.55, 9.13, 9.54 and 9.73 min, with the protonated molecular ions at *m/z* 595.165, 595.1668, 595.1649 and 595.1667 ($C_{27}H_{30}O_{16}$, mass error <1.76 ppm), respectively. Their $[M+H]^+$ ions were 176 Da (GluA) higher than those of M1, and the MS^2 spectra (generated from the *m/z* 595.17 precursor) exhibited fragmentation patterns consistent with M1. Therefore, they were tentatively identified as glucuronide conjugates of M1. Moreover, some crucial fragment ions at *m/z* 389.0866, 374.0631, 346.0685, 197.0084 ($^{1,3}A^+$), 178.0627 ($^{1,3}B^+$), 169.0142 ($^{1,3}A^+$), 165.0547 ($^{0,2}B^+$) were consistent with the fragment ions of HMF-A1 metabolites, which were yielded by dropping $C_6H_8O_6$ and then successively losing $2\cdot CH_3$, $\cdot CH_3$ and CO as well as the RDA reaction based on the ion *m/z* 389.0866. Consequently, M6-1, M6-2, and M6-4 were tentatively identified as glucuronidated conjugates of HMF-A1

(HMF-A1+GluA). In contrast, M6-3 exhibited a fragment ion profile matching that of B-ring mono-demethylated metabolites (HMF-B1) after the loss of the glucuronide group, leading to its tentative identification as a glucuronide conjugate of HMF-B1 (HMF-B1+GluA). It should be noted that the specific position of glucuronide attachment on the flavonoid skeleton could not be determined in this study due to the absence of diagnostic fragment ions retaining the glucuronide group.

3.4.7 Glucuronide conjugates of dihydroxy-pentamethoxyflavone (M7)

Metabolites M7-1 to M7-6 were detected at 7.74, 7.96, 8.25, 9.49, 9.85 and 11.81 min, respectively. They had similar protonated ions at *m/z* 581.1490, 581.1490, 581.1490, 581.1492, 581.1492 and 581.1493 ($C_{26}H_{28}O_{15}$, mass error <1.89 ppm), respectively, which were 176 Da higher than those of M2. In the MS^2 spectra, M7-1, M7-2, M7-3, M7-5 and M7-6 possessed several representative fragment ions at *m/z* 375.0708, 360.0474, 347.0754, 197.0080, 169.0130, 164.0465 and 151.0388. This fragmentation profile is consistent with that of the A- and B-ring mono-demethylated metabolites (HMF-A1B1), indicating that these five isomers were glucuronidated derivatives of HMF-A1B1 (HMF-A1B1+GluA). In contrast, metabolite M7-4 exhibited DPIs matching those of the B-ring di-demethylated metabolite. Consequently, M7-4 was tentatively identified as the glucuronide conjugate of 3′,4′-dihydroxy-3,5,6,7,8-pentamethoxyflavone (HMF-B2+GluA).

3.4.8 Glucuronide conjugates of trihydroxy-tetramethoxyflavone (M8)

Metabolites M8-1 to M8-9, which had the same element composition as $C_{25}H_{26}O_{15}$, yielded protonated molecular ions at *m/z* 567.1341, 567.1335, 567.1337, 567.1337, 567.1345, 567.1328, 567.134, 567.1336 and 567.1345 (mass error <2.91 ppm), respectively. Their $[M+H]^+$ ions were 176 Da greater than those of M3, indicating that glucuronide conjugation occurred after losing three methyl groups. With the exception of M8-6, all M8 metabolites exhibited DPIs identical to those of HMF-A1B2, supporting their identification as glucuronide conjugates of HMF-A1B2 (HMF-A1B2+GluA). In contrast, M8-6 displayed the DPIs profile consistent with HMF-A2B1, identifying it as the corresponding glucuronidated derivative (HMF-A2B1+GluA).

3.5 Semiquantitative analysis of demethylated metabolites of HMF

The HREIC of HMF metabolites in urine, feces and plasma without or with enzymatic treatment are shown in Figure 5, Figure S1 and Figure S2, respectively. Most metabolites were detected in urine and feces, and only a few were detected in plasma. There were both free and conjugated forms of demethylated metabolites in plasma and urine, while most of the metabolites in feces are free forms. It is notable that a greater number of demethylated metabolites were found after pre-treating with enzymatic hydrolysis by glucuronidase and sulfatase, suggesting that they (e.g., M1-2, M1-4 and M1-5) exist as conjugated forms in the plasma (Figure 5B and Figure S1B). In order to comprehensively understand the metabolic profile of HMF, we analyzed the relative abundance of HMF and its all demethylated metabolites in the plasma, urine and feces with enzymatic treatment by using the area normalization method (Figure 6-8). As shown in Figure 6, the relative abundance of HMF in the plasma gradually decreased from 27.74% to 6.13% within 10 hours

post-administration but disappeared after 10 h. HMF underwent extensive metabolism, producing a series of demethylated metabolites. Within the first 10 hours, M1 constituted the predominant metabolite (over 70.6%), succeeded by M2 (54.8%) at 24 hours and M3 (over 39.9%) beyond 24 hours, reflecting a time-dependent shift toward more extensively demethylated species and indicating enhanced sequential demethylation activity over time in the systemic circulation. Furthermore, A-ring demethylated metabolites consistently exhibited higher relative abundances than their B-ring counterparts, suggesting a preferential demethylation site on the A-ring of HMF in blood. For the specific metabolite, the most abundant metabolite was M1-3 within 10 hours (over 28.7%), followed by M2-1 (34.5%) at 24 hours and M3-2 after 24 hours (over 39.9%).

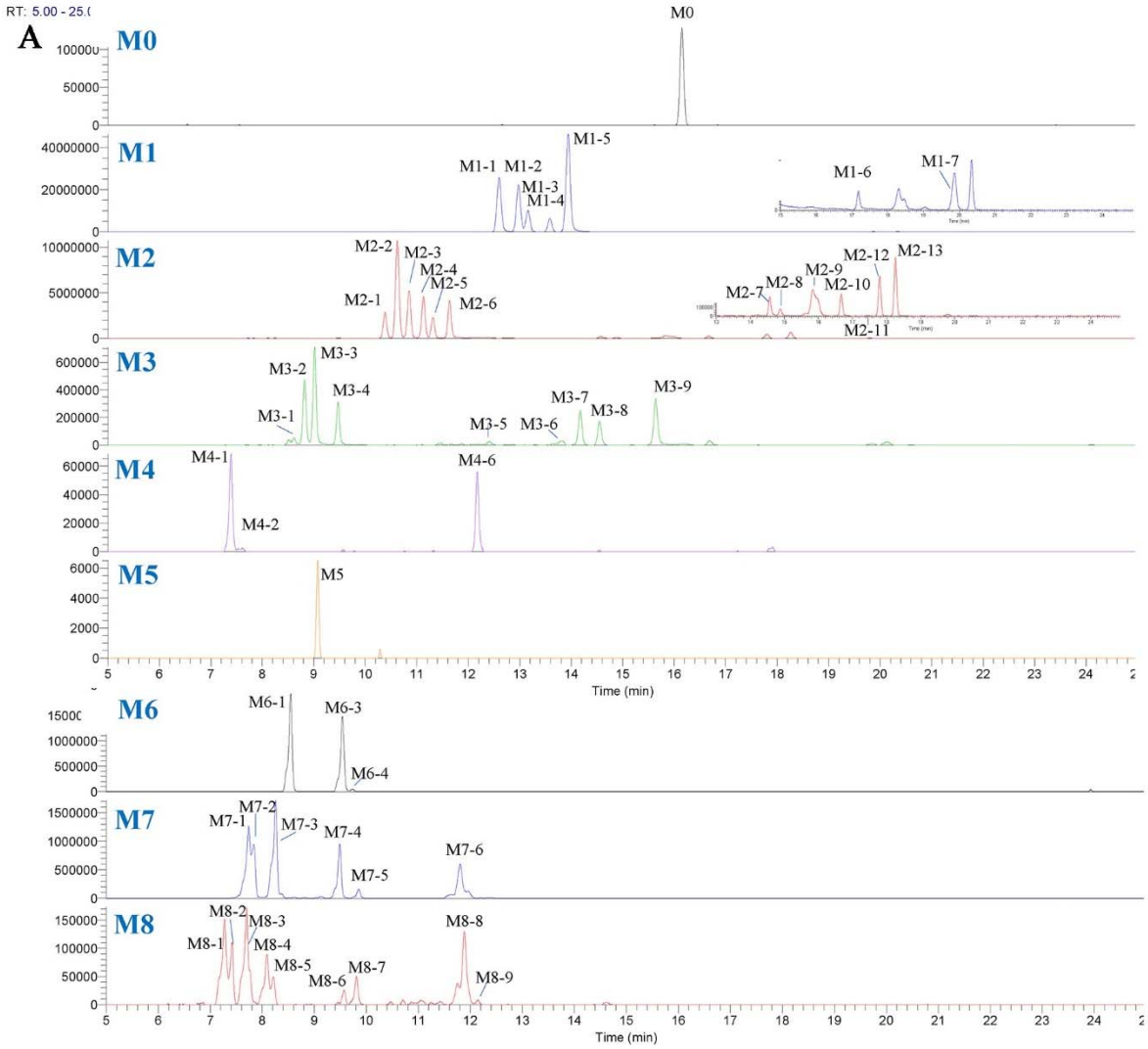

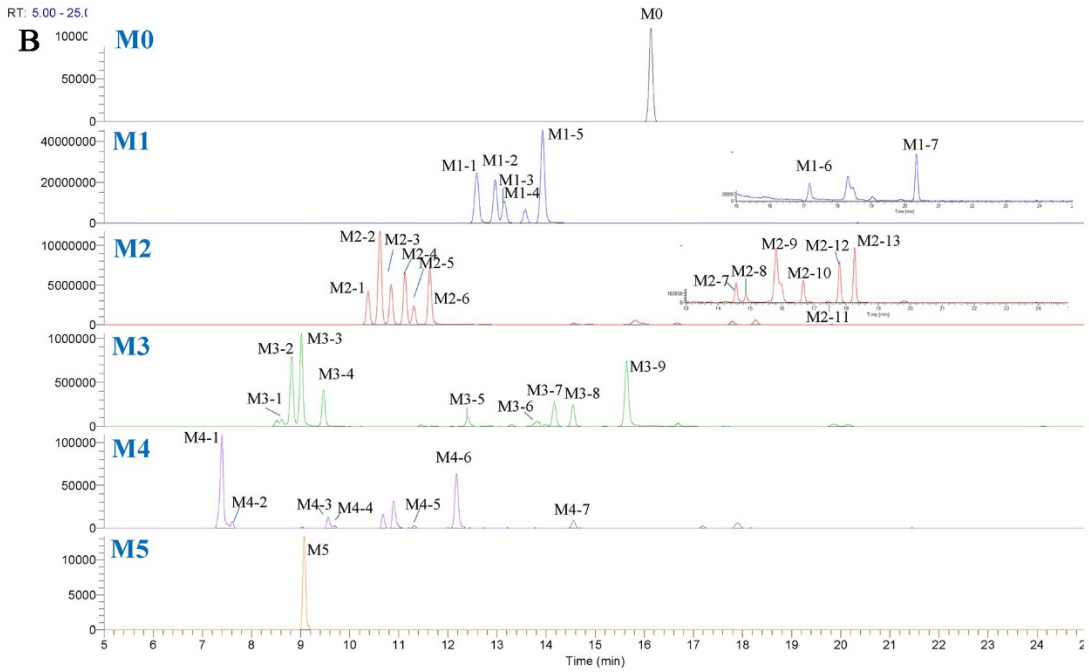

Figure 5. High-resolution extracted ion chromatograms (HREIC) of HMF metabolites in urine (A) before and (B) after enzymatic hydrolysis. Detected metabolites are categorized as follows: M0 (parent HMF); M1-1 to M1-7 (monohydroxy-hexamethoxyflavone); M2-1 to M2-13 (dihydroxy-pentamethoxyflavone); M3-1 to M3-9 (trihydroxy-tetramethoxyflavone); M4-1 to M4-7 (tetrahydroxy-trimethoxyflavone); M5 (pentahydroxy-dimethoxyflavone); M6-1 to M6-4 (glucuronide conjugates of monohydroxy-hexamethoxyflavone); M7-1 to M7-6 (glucuronide conjugates of dihydroxy-pentamethoxyflavone); M8-1 to M8-9 (glucuronide conjugates of trihydroxy-tetramethoxyflavone). Detailed information for all metabolites is listed in Table 1.

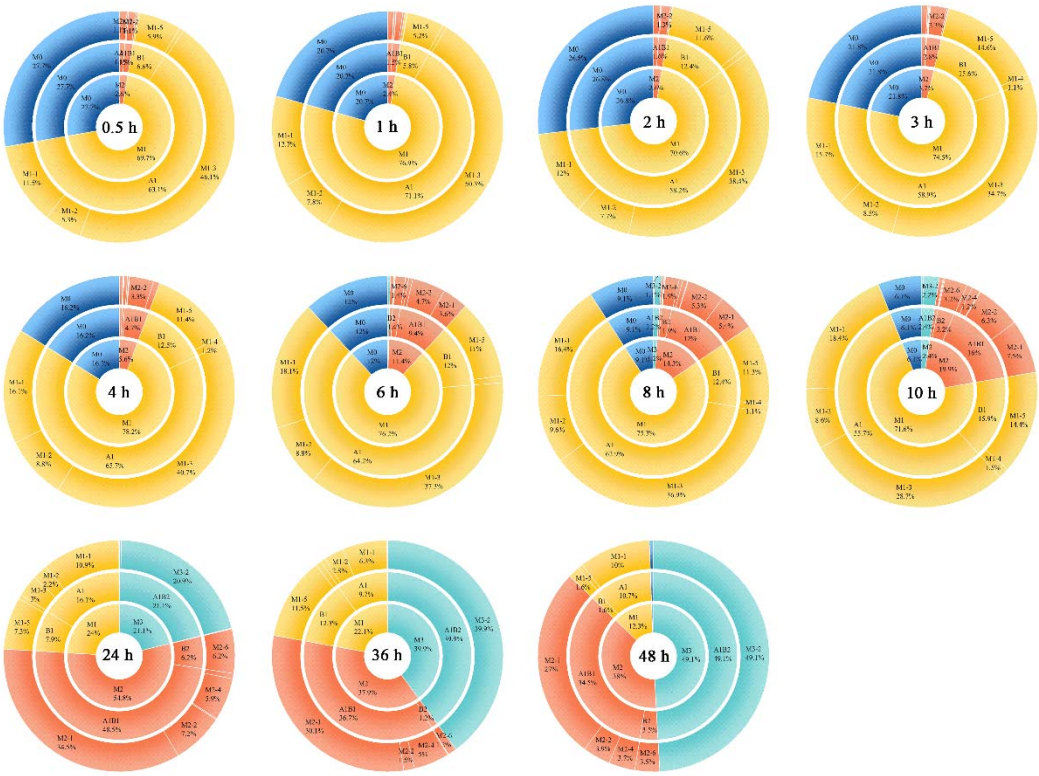

Figure 6. Relative abundance of HMF and its demethylated metabolites in enzymatically hydrolyzed plasma at different time points after oral administration of 45 mg/kg HMF. The data are visualized in a sunburst chart, where the inner ring categorizes metabolites (M0-M5) by the number of demethylation events, the middle ring shows subcategories based on the demethylation site (A-, B-, or C-ring), and the outer ring specifies individual metabolites. M1–M5 denote mono-, di-, tri-, tetra-, and penta-demethylated metabolites, respectively. For subcategories, the letter denotes the ring and the digit signifies the number of demethylations. A complete list of individual metabolites is provided in Table 1.

Figure 7 illustrates that more than 99% of HMF underwent demethylation after absorption, with M1 being the predominant metabolite in urine. The metabolic profile shifted following a single-dose PO, where the abundance of M1 gradually decreased from 97% to 80.8% over 48 hours, while the levels of M2 and M3 increased. A similar metabolic trend was maintained following consecutive oral administration from day 3 to day 7. Notably, the diversity of demethylated metabolites increased by day 7. Additionally, the relative abundance of certain di-demethylated metabolites, such as M2-2, M2-4, and M2-6, significantly increased over time. These findings indicate that repeated HMF administration enhanced its biotransformation, thereby promoting the production of a more diverse array of demethylated metabolites. Consistent with its biotransformation in blood, HMF demethylation in urine occurred predominantly on the A-ring. The relative abundance of specific metabolites shifted from M1-1 (＞27.3%), which was dominant within 48 hours after a single dose, to M1-5 (24.4%), which became the predominant metabolite following consecutive dosing by day 7.

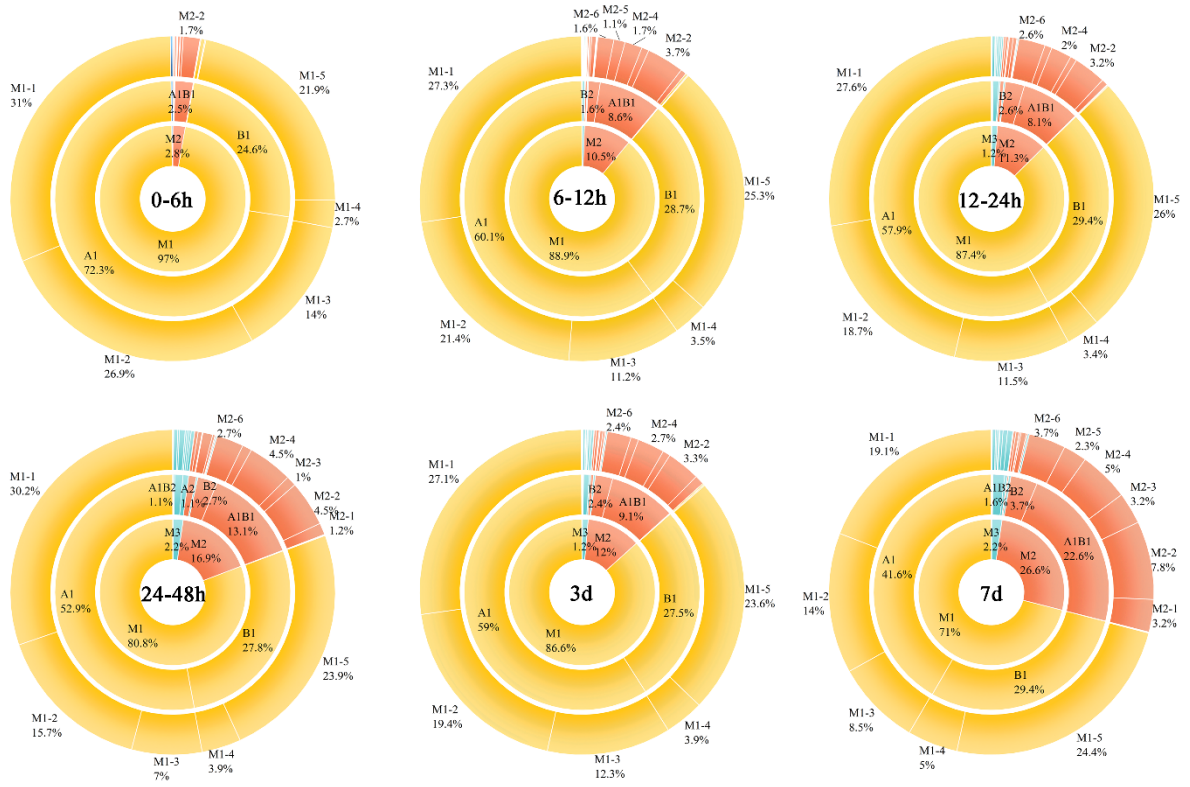

Figure 7. Relative abundance of HMF and its demethylated metabolites in enzymatically hydrolyzed urine following single or consecutive oral administration of HMF (45 mg/kg). Urine was collected at 6, 12, 24, and 48 hours post single dose, and on days 3 and 7 during consecutive administration.

As shown in Figure 9, over 99% of HMF was metabolized in feces, with M1 being the dominant metabolite. Following a single-dose PO, the relative abundance of M1 significantly decreased from 77.6% to 41.8%. Notably, fecal excretion demonstrated a greater capacity for sequential demethylation than urinary excretion, evidenced by the concomitant rise in M2 (22.7%), M3 (28.1%), and M4 (6.6%) abundances within 24–48 h. Furthermore, the diversity of demethylated metabolites increased over time after a single dose, a trend that persisted throughout the consecutive dosing period from days 3 to 7. By day 7, the abundances of

most M2, M3, and M4 metabolites were elevated. Notably, M1-5 emerged as the most abundant metabolite (15.5%), followed by M1-1 (14.5%), M2-2 (8.6%), M2-6 (8.1%), and M3-2 (7.2%).

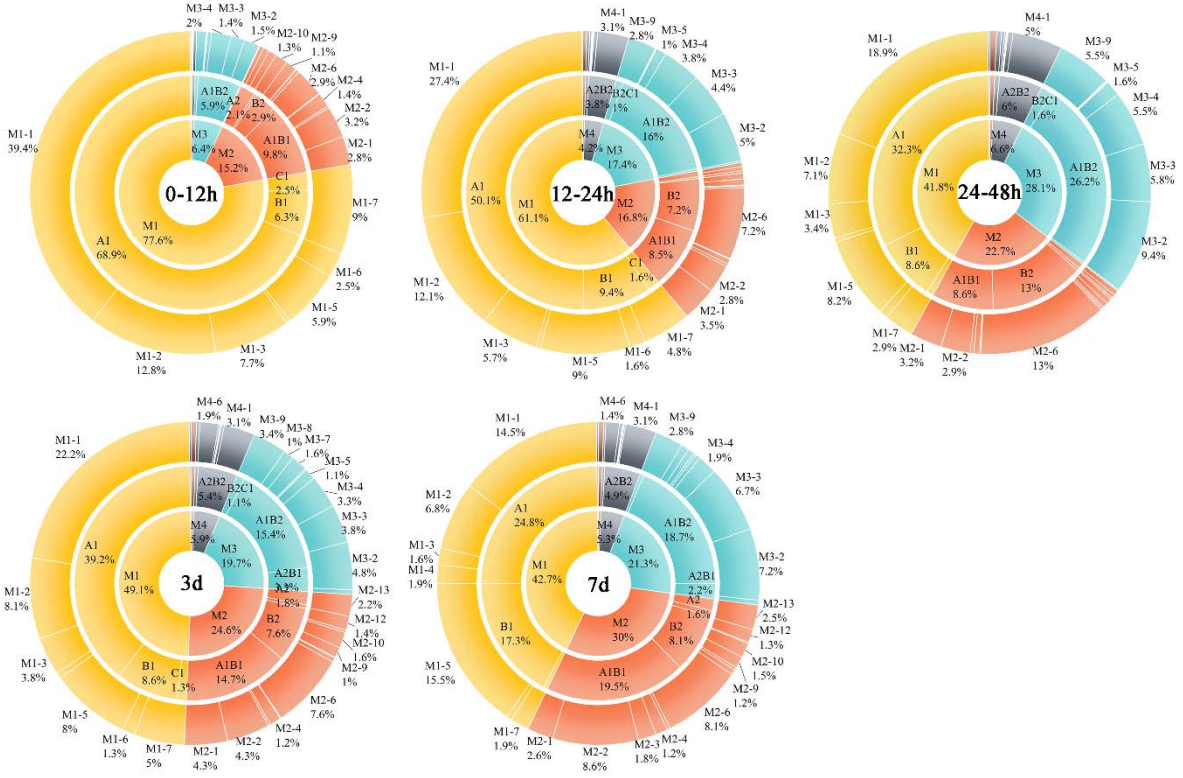

Figure 8. Relative abundance of HMF and its demethylated metabolites in enzymatically hydrolyzed feces following single or consecutive oral administration of HMF (45 mg/kg). Fecal sample was collected at 12, 24, and 48 hours post single dose, and on days 3 and 7 during consecutive administration.

3.6 Possible biotransformation pathways of HMF

The chemical structures of all identified HMF metabolites *in vivo* are summarized in Figure 9A. Based on the metabolite identification and semi-quantitative analysis, the potential biotransformation pathways of HMF in rats are proposed in Figure 9B. HMF was first mono-demethylated to form seven distinct M1 metabolites. These M1 metabolites subsequently underwent sequential demethylation, leading to the formation of multiple di- (M2), tri- (M3), tetra- (M4), and penta-demethylated metabolites (M5). Concurrently, the demethylated metabolites (M1–M3) were subject to glucuronide conjugation. Overall, the results indicate that the metabolism of HMF in rats proceeds primarily through a series of demethylation reactions, followed by glucuronidation.

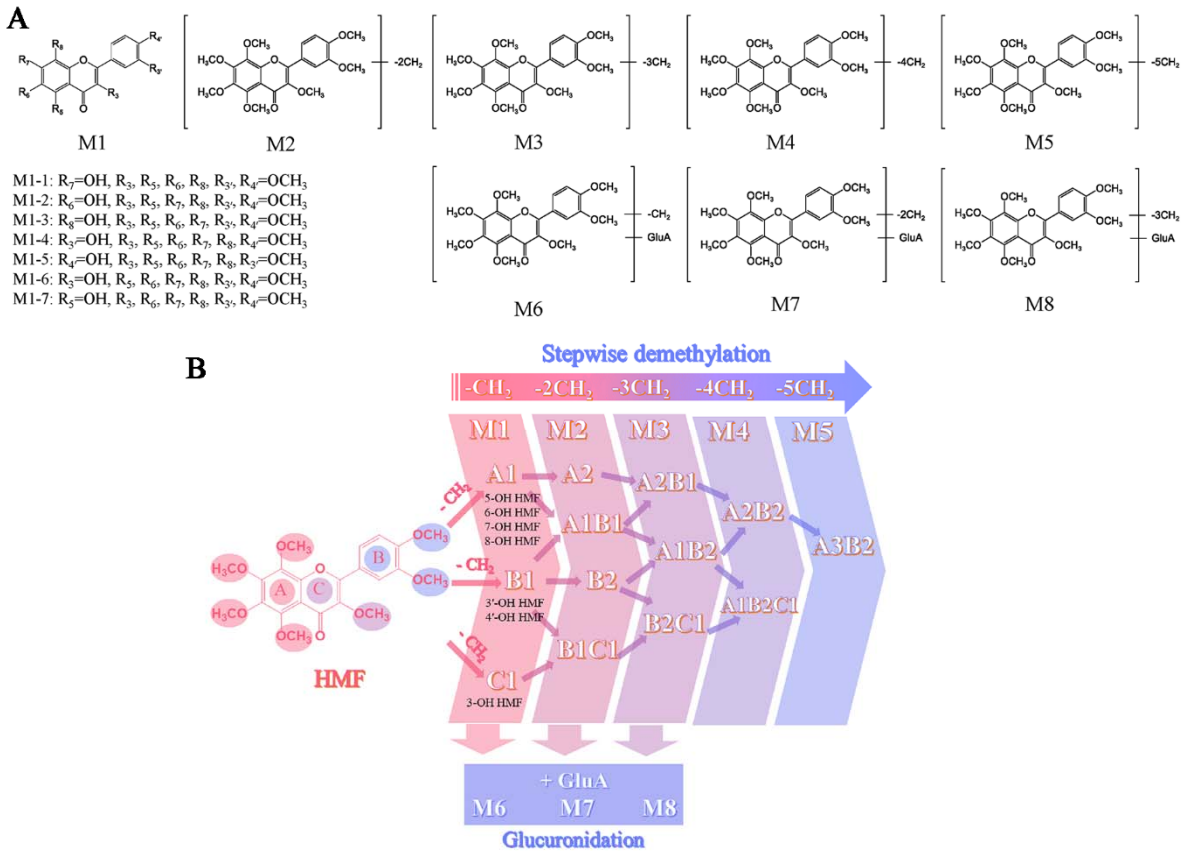

Figure 9. (A) Chemical structures of the *in vivo* metabolites of HMF. (B) Proposed metabolic pathways of HMF *in vivo*. Metabolites are denoted as follows: M1–M5, mono- to penta-demethylated metabolites; M6–M8, glucuronide conjugates of mono-, di-, and tri-demethylated metabolites, respectively. The prefixes A, B, and C designate the three aromatic rings of HMF, with the subsequent digit indicating the number of demethylation events on that ring. GluA, glucuronic acid.

4. Discussion

The *in vivo* metabolism of drugs or bioactive compounds is crucial for understanding their pharmacological safety and efficacy. However, the inherent complexity of metabolic processes poses significant challenges for comprehensive metabolite identification. In recent years, the emergence of various analytical technologies, including UPLC technology, HRMS and data processing software, have substantially enhanced our capability to characterize *in vivo* metabolites[39, 40]. For example, Li et al.[23] identified a total of 106 metabolites of ononin in rats using UHPLC-HRMS/MS coupled with advanced data-processing methods, while Wang et al.[41] characterized 39 metabolites of amentoflavone in both *in vivo* and *in vitro*. In this study, a total of 56 HMF metabolites in rat biological samples were characterized using UHPLC-LTQ-Orbitrap HRMS/MS analysis combined with enzymatic hydrolysis pretreatment and multiple data acquisition/processing approaches. In order to further structurally distinguish these metabolites, we employed RDA fragmentation patterns from MS^2 spectra to determine the distribution of hydroxyl and methoxy substituents on the A-, B-, and C-rings of HMF metabolites (Table 1). However, due to the presence of multiple isomers and the absence of reference standards, we were not able to precisely confirm the chemical structures of di-, tri-, tetra-, and penta-demethylated metabolites of HMF. Future research should focus on metabolite isolation or the application of complementary analytical techniques (e.g., NMR) to achieve definitive structural confirmation.

Previous *in vivo* biotransformation studies of PMFs, including nobiletin, tangeretin, and sinensetin, have demonstrated that these compounds primarily underwent phase I metabolism to product demethylated metabolites and phase II metabolism to form sulfate/glucoronidate conjugates[17, 20, 25]. Early study has found 10 tangeretin metabolites in urine and fecal samples, with seven structurally characterized using LC/MS and ^{1}H NMR, including 4′- and 6-demethyltangeretin, 3′,4′-, 4′,7-, 4′,6-, and 5,6- dihydroxylnobiletin, and 4′,6,7-tridemethyltangeretin[20]. Moreover, seven metabolites of nobiletin, including 3′-, 4′-, and 5-demethylnobiletin, 3′,4′-, 5,3′- and 5,4′- demethylnobiletin and 5,3′,4′-tridemethylnobiletin, were discovered in the mouse urine[42]. Notably, a recent study identified all six mono-demethylated metabolites of nobiletin in rat plasma and tissues, including the first reported detection of 8-demethylnobiletin along with confirmed *in vivo* presence of 6- and 7-demethylnobiletin. In contrast to these well-characterized PMFs, reports on HMF metabolites remain limited, with only a few mono- and di-demethylated metabolites and their glucuronide conjugates described, and no comprehensive structural elucidation[13, 14]. The present study systematically characterized 56 HMF metabolites in plasma, urine, and feces using UHPLC-HRMS/MS, including 37 free-formed demethylated metabolites (7 mono-, 13 di-, 9 tri-, 7 tetra-, and 1 penta-demethylated) and 19 their glucuronide conjugates (Table 1). Notably, all seven mono-demethylated metabolites of HMF were simultaneously found and structurally distinguish for the first time in rats, and most of these diverse metabolites have not previously been described as *in vivo* metabolites of HMF. Moreover, the metabolic profile of HMF exhibited greater diversity than other PMFs (e.g., nobiletin and tangeretin)[19, 20], likely due to its higher number of methoxy groups.

To elucidate the overall metabolic fate of HMF, the relative abundance of its demethylated metabolites in plasma, urine and feces was analyzed by the area normalization method. The results indicated that HMF underwent extensive demethylated biotransformation in rats. Both single-dose and consecutive-dose studies demonstrated a time-dependent decrease in M1 abundance, accompanied by increased levels of M2-M4 metabolites, suggesting enhance demethylation activity over time. Based on metabolite identification and semi-quantitative analysis, we proposed that the metabolism of HMF progressed through an initial mono-demethylation, yielding seven distinct M1 metabolites, followed by their sequential demethylation into various M2-M5 metabolites, as well as glucuronide conjugates. In addition, although similar metabolic pathways of HMF were observed across blood, urine and feces, notable differences emerged in metabolite diversity and abundance. Fecal samples contained a more diverse array of demethylated metabolites, particularly M3-M5 species, compared to the plasma and urinary samples. Moreover, fecal excretion exhibited significantly higher demethylation activity than urinary excretion, as indicated by the greater relative abundances of M2-M4 metabolites. These findings suggested that gut microbiota might possess stronger demethylation capacity than host metabolic systems, consistent with previous observations for nobiletin[43]. Notably, a further novel finding of this study is the identification of A-ring demethylation as the predominant metabolic pathway for HMF *in vivo*. This result is inconsistent with previous reports on other PMFs, such as nobiletin and tangeretin, which indicated a preference for demethylation at the C-4′ position of

the B-ring[17, 20, 38, 42]. Two factors might account for this observed discrepancy. First, the present study simultaneously identified and relatively quantified a greater number of A-ring demethylated metabolites, particularly mono-demethylated metabolites, compared to earlier reports on nobiletin and tangeretin. These findings aligned with a recent investigation highlighting the A ring of nobiletin as the principal site of demethylation following a single oral administration, based on quantitative analysis of all monodemethylnobiletin isomers[37]. Second, dosing duration might affect metabolic patterns. Previous investigations often used long-term feeding to maximize metabolic effects[17, 20], whereas this study employed both single-dose and short-term (5 days) consecutive administration. While this study provides initial insights into the *in vivo* metabolism of HMF, the proposed biotransformation pathway requires further validation in our ongoing long-term dosing study. Moreover, subsequent investigations should employ absolute quantification to precisely delineate these metabolic pathways.

5. Conclusion

This study presents the first comprehensive characterization of the *in vivo* metabolic profile of HMF in rats, with 56 metabolites identified in urine, feces, and plasma. Notably, all seven mono-demethylated metabolites were simultaneously detected and structurally characterized for the first time after oral dosing. Metabolic profiling revealed that HMF was first metabolized to form mono-demethylated metabolites, followed by progressive sequential demethylation to form di-, tri-, tetra-, and penta-demethylated metabolites, as well as glucuronide conjugates. These results elucidated demethylation and glucuronidation as the primary metabolic pathways of HMF, which provided critical insights into further pharmacological studies of HMF and established a valuable methodology for metabolic characterization of other PMFs.

Acknowledgements

This work was financially supported by National Natural Science Foundation of China (32472353), Youth Innovation Talent Projects of Higher Education Institution in Guangdong Province (2024KQNCX146), Guangdong Basic and Applied Basic Research Foundation (2024A1515110085), Guangdong Provincial Key Laboratory of Nutraceuticals and Functional Foods (2018B030322010) and Program for Guangdong Introducing Innovative and Entrepreneurial Teams (2019ZT08N291).

Declaration of competing interest

The authors declare that they have no known competing financial interests or personal relationships that could have appeared to influence the work reported in this paper.

References

[1] A.I. Owis, Citrus polymethoxyflavones: biofunctional molecules of therapeutic interest, Stud. Nat. Prod. Chem. 59 (2018) 509-530. https://doi.org/10.1016/b978-0-444-64179-3.00015-3.

[2] Z. Gao, W. Gao, S.-L. Zeng, et al., Chemical structures, bioactivities and molecular mechanisms of citrus polymethoxyflavones, J. Funct. Foods. 40 (2018) 498-509. https://doi.org/10.1016/j.jff.2017.11.036.

[3] L. Duan, L.L. Dou, K.Y. Yu, et al., Polymethoxyflavones in peel of Citrus reticulata 'Chachi' and their biological activities, Food Chem. 234 (2017) 254-261. https://doi.org/10.1016/j.foodchem.2017.05.018.

[4] A. Sawamoto, M. Nakanishi, S. Okuyama, et al., Heptamethoxyflavone inhibits adipogenesis via enhancing PKA signaling, Eur J Pharmacol. 865 (2019) 172758. https://doi.org/10.1016/j.ejphar.2019.172758.

[5] S. Okuyama, K. Miyazaki, R. Yamada, et al., Permeation of polymethoxyflavones into the mouse brain and their effect on MK-801-induced locomotive hyperactivity, Int. J. Mol. Sci. 18 (2017) 489. https://doi.org/10.3390/ijms18030489.

[6] P.T. Xiao, Z.S. Xie, Y.J. Kuang, et al., Discovery of a potent FKBP38 agonist that ameliorates HFD-induced hyperlipidemia via mTOR/P70S6K/SREBPs pathway, Acta Pharm. Sin. B. 11 (2021) 3542-3552. https://doi.org/10.1016/j.apsb.2021.03.031.

[7] K. Feng, X. Zhu, T. Chen, et al., Prevention of obesity and hyperlipidemia by heptamethoxyflavone in high-fat diet-induced rats, J. Agric. Food Chem. 67 (2019) 2476-2489. https://doi.org/10.1021/acs.jafc.8b05632.

[8] K. Feng, H. Zhang, C. Chen, et al., Heptamethoxyflavone alleviates metabolic syndrome in high-fat diet-fed mice by regulating the composition, function, and metabolism of gut microbiota, J. Agric. Food Chem. 71 (2023) 10050-10064. https://doi.org/10.1021/acs.jafc.3c01881.

[9] X. Wu, M. Song, M. Wang, et al., Chemopreventive effects of nobiletin and its colonic metabolites on colon carcinogenesis, Mol. Nutr. Food Res. 59 (2015) 2383-2394. https://doi.org/10.1002/mnfr.201500378.

[10] J. Zheng, M. Song, P. Dong, et al., Identification of novel bioactive metabolites of 5-demethylnobiletin in mice, Mol. Nutr. Food Res. 57 (2013) 1999-2007. https://doi.org/10.1002/mnfr.201300211.

[11] S. Guo, X. Wu, J. Zheng, et al., Identification of 4′-demethyltangeretin as a major urinary metabolite of tangeretin in mice and its anti-inflammatory activities, J. Agric. Food Chem. 69 (2021) 4381-4391. https://doi.org/10.1021/acs.jafc.0c06334.

[12] X.A. Zhu, G.Y. Ding, S.C. Ren, et al., The bioavailability, absorption, metabolism, and regulation of glucolipid metabolism disorders by quercetin and its important glycosides: A review, Food Chem. 458 (2024) 140262. https://doi.org/10.1016/j.foodchem.2024.140262.

[13] M. Nery, P.S. Ferreira, D.R. Goncalves, et al., Physiological effects of tangeretin and heptamethoxyflavone on obese C57BL/6J mice fed a high-fat diet and analyses of the metabolites originating from these two polymethoxylated flavones, Food Sci. Nutr. 9 (2021) 1997-2009. https://doi.org/10.1002/fsn3.2167.

[14] J.A. Manthey, P. Bendele, Anti-inflammatory activity of an orange peel polymethoxylated flavone, 3′,4′,3,5,6,7,8-heptamethoxyflavone, in the rat carrageenan/paw edema and mouse lipopolysaccharide-challenge assays, J. Agric. Food Chem. 56 (2008) 9399-9403.

[15] A. Karn, C. Zhao, F. Yang, et al., In-vivo biotransformation of citrus functional components and their effects on health, Crit. Rev. Food Sci. Nutr. 61 (2021) 756-776. https://doi.org/10.1080/10408398.2020.1746234.

[16] M. Wang, H. Zhao, X. Wen, et al., Citrus flavonoids and the intestinal barrier: Interactions and effects, Compr. Rev. Food Sci. Food Saf. 20 (2021) 225-251. https://doi.org/10.1111/1541-4337.12652.

[17] S. Li, Z. Wang, S. Sang, et al., Identification of nobiletin metabolites in mouse urine, Mol. Nutr. Food Res. 50 (2006) 291-299. https://doi.org/10.1002/mnfr.200500214.

[18] N. Koga, C. Ohta, Y. Kato, et al., In vitro metabolism of nobiletin, a polymethoxy-flavonoid, by human liver microsomes and cytochrome P450, Xenobiotica. 41 (2011) 927-933. https://doi.org/10.3109/00498254.2011.593208.

[19] S. Li, H. Wang, L. Guo, et al., Chemistry and bioactivity of nobiletin and its metabolites, J. Funct. Foods. 6 (2014) 2-10. https://doi.org/10.1016/j.jff.2013.12.011.

[20] S. Nielsen, V. Breinholt, C. Cornett, et al., Biotransformation of the citrus flavone tangeretin in rats. Identification of metabolites with intact flavane nucleus, Food Chem Toxicol. 38 (2000) 739-746. https://doi.org/https://doi.org/10.1016/S0278-6915(00)00072-7.

[21] Z.T.A. Shakour, N.M. Fayek, M.A. Farag, How do biocatalysis and biotransformation affect Citrus dietary flavonoids chemistry and bioactivity? A review, Crit Rev Biotechnol. 40 (2020) 689-714. https://doi.org/10.1080/07388551.2020.1753648.

[22] X. Wang, D. Li, Y. Cao, et al., Identification and quantification of both methylation and demethylation biotransformation metabolites of 5-demethylsinensetin in rats, J. Agric. Food Chem. 70 (2022) 3162-3171. https://doi.org/10.1021/acs.jafc.1c07509.

[23] H.F. Li, T. Li, P. Yang, et al., Global profiling and structural characterization of metabolites of ononin using HPLC-ESI-IT-TOF-MS(n) after oral administration to rats, J. Agric. Food Chem. 68 (2020) 15164-15175. https://doi.org/10.1021/acs.jafc.0c04247.

[24] H. Zhou, S. Song, X. Lan, et al., Comprehensive profiling of mangiferin metabolites in vivo and in vitro based on the "drug metabolite clusters" analytical strategy, ACS Omega. (2023) https://doi.org/10.1021/acsomega.2c07089.

[25] X. Wang, D. Li, Y. Cao, et al., Biotransformation and quantification of sinensetin and its metabolites in plasma, urine, and feces of rats, J. Agric. Food Chem. 69 (2021) 14143-14150. https://doi.org/10.1021/acs.jafc.1c05024.

[26] M. Luo, Y. Han, Y. Chen, et al., Unveiling the role of gut microbiota in curcumin metabolism using antibiotic-treated mice, Food Chem. 460 (2024) 140706. https://doi.org/10.1016/j.foodchem.2024.140706.

[27] Y. Ding, M. Peng, T. Zhang, et al., Quantification of conjugated metabolites of drugs in biological matrices after the hydrolysis with beta-glucuronidase and sufatase: a review of bio-analytical methods, Biomed Chromatogr. 27 (2013) 1280-1295. https://doi.org/10.1002/bmc.2912.

[28] H. Henry, H.R. Sobhi, O. Scheibner, et al., Comparison between a high-resolution single-stage Orbitrap and a triple quadrupole mass spectrometer for quantitative analyses of drugs, Rapid Commun. Mass Spectrom. 26 (2012) 499-509. https://doi.org/10.1002/rcm.6121.

[29] N.R. Zhang, S. Yu, P. Tiller, et al., Quantitation of small molecules using high-resolution accurate mass spectrometers - a different approach for analysis of biological samples, Rapid Commun. Mass Spectrom. 23 (2009) 1085-1094. https://doi.org/10.1002/rcm.3975.

[30] X. Chen, L. Xu, S. Guo, et al., Profiling and comparison of the metabolites of diosmetin and diosmin in rat urine, plasma and feces using UHPLC-LTQ-Orbitrap MS(n), J. Chromatogr. B Analyt. Technol. Biomed. Life Sci. 1124 (2019) 58-71. https://doi.org/10.1016/j.jchromb.2019.05.030.

[31] J. Yin, Y. Ma, C. Liang, et al., A systematic study of the metabolites of dietary acacetin in vivo and in vitro based on UHPLC-Q-TOF-MS/MS analysis, J. Agric. Food Chem. 67 (2019) 5530-5543. https://doi.org/10.1021/acs.jafc.9b00330.

[32] J. Yin, X. Zhang, Y. Zhang, et al., Comprehensive study of the in vivo and in vitro metabolism of dietary isoflavone biochanin A based on UHPLC-Q-TOF-MS/MS, J. Agric. Food Chem. 67 (2019) 12481-12495. https://doi.org/10.1021/acs.jafc.9b05776.

[33] L. Chen, H. Cao, Q. Huang, et al., Absorption, metabolism and bioavailability of flavonoids: a review, Crit. Rev. Food Sci. Nutr. 62 (2022) 7730-7742. https://doi.org/10.1080/10408398.2021.1917508.

[34] Y. Liu, X. Zhao, C. Wang, et al., Metabolism, distribution, and excretion of ethanamizuril in chickens, J. Agric. Food Chem. 68 (2020) 1563-1570. https://doi.org/10.1021/acs.jafc.9b05065.

[35] X. Yu, D. Li, Y. Yu, et al., Characterization of free and bound polymethoxyflavones in the dried peel of Citrus reticulata "Chachi" through fingerprint RDA ions and reversed-phase column retention by UPLC-Q-TOF-MS/MS, Food Chem. 471 (2025) https://doi.org/10.1016/j.foodchem.2025.142831.

[36] T.T. Xing, X.J. Zhao, Y.D. Zhang, et al., Fast separation and sensitive quantitation of polymethoxylated flavonoids in the peels of citrus using UPLC-Q-TOF-MS, J. Agric. Food Chem. 65 (2017) 2615-2627. https://doi.org/10.1021/acs.jafc.6b05821.

[37] M. Iwashita, R. Shioi, M. Sugiyama, et al., Monodemethylated metabolites of orally administered nobiletin: Identification and quantitation in rat plasma and tissues, J. Agric. Food Chem. 71 (2023) 10028-10036. https://doi.org/10.1021/acs.jafc.3c00096.

[38] M. Zhang, Y. Xin, K. Feng, et al., Comparative analyses of bioavailability, biotransformation and excretion of nobiletin in lean and obese rats, J. Agric. Food Chem. 68 (2020) 10709-10718. https://doi.org/10.1021/acs.jafc.0c04425.

[39] H. Wang, J. Xu, P. Dong, et al., Comprehensive analysis of pterostilbene metabolites in vivo and in vitro using a UHPLC-Q-exactive plus mass spectrometer with multiple data-mining methods, ACS Omega. 7 (2022) 38561-38575. https://doi.org/10.1021/acsomega.2c03924.

[40] J. Huang, S. Huang, J. Zhang, et al., A systematic strategy for the characterization of 2,3,5,4'-tetrahydroxystilbene-2-O-beta-d-glucoside metabolites in vivo by ultrahigh performance liquid chromatography coupled with a Q Exactive-Orbitrap mass system, J. Agric. Food Chem. 70 (2022) 7773-7785. https://doi.org/10.1021/acs.jafc.2c00572.

[41] B. Wang, Y. Lu, X. Hu, et al., Systematic strategy for metabolites of amentoflavone in vivo and in vitro based on UHPLC-Q-TOF-MS/MS analysis, J. Agric. Food Chem. 68 (2020) 14808-14823. https://doi.org/10.1021/acs.jafc.0c04532.

[42] J. Zheng, J. Bi, D. Johnson, et al., Analysis of 10 metabolites of polymethoxyflavones with high sensitivity by electrochemical detection in high-performance liquid chromatography, J. Agric. Food Chem. 63 (2015) 509-516. https://doi.org/10.1021/jf505545x.

[43] M. Zhang, X. Zhang, J. Zhu, et al., Bidirectional interaction of nobiletin and gut microbiota in mice fed with a high-fat diet, Food Funct. 12 (2021) 3516-3526. https://doi.org/10.1039/d1fo00126d.